https://doi.org/10.15407/ufm.25.04.661

N.M. BILYAVYNA[1,*], V.Z. TURKEVYCH[2,], D.A. STRATIICHUK[2,***], A.M. KURYLIUK[1,****], and O.I. NAKONECHNA[1,*****]**

[1] Taras Shevchenko National University of Kyiv,
64/13, Volodymyrska Str., 01601 Kyiv, Ukraine
[2] V.M. Bakul Institute for Superhard Materials of the N.A.S. of Ukraine,
2 Avtozavodska Str., 04074 Kyiv, Ukraine

* nbelyavina@ukr.net, ** vturk@ism.kiev.ua, *** d_strat@ukr.net,
**** alla.kuryliuk@knu.ua, ***** lesnak4@gmail.com

ON THE FORMATION OF SOLID SOLUTIONS AT THERMOBARIC SINTERING OF PcBN COMPOSITES OF cBN–*Me*N–Al AND cBN–*Me*C–Al SYSTEMS

Using the x-ray diffraction method, we study in detail a series of polycrystalline cubic boron nitride (PcBN) composites of the cBN–{TiN, ZrN, HfN, VN, NbN}–Al and cBN–{TiC, ZrC, HfC, VC, NbC, TaC}–Al systems (with a charge composition of 60:35:5 vol.%) sintered at high pressures and high temperatures (HPHT): 7.7 GPa, 1600–2450 °C. As shown, the crystal structure of each nitride *Me*N or carbide *Me*C (*Me* = Ti, Zr, Hf, V, Nb, Ta) existing in these composites belongs to a modified NaCl-type structure with the additional position for nitrogen atoms that results in the accumulation of N-atoms' excess in the near-surface layers of composites. Al atoms of the charge are embedded into the *Me*C crystal lattice at certain sintering temperatures forming substitutional solid solutions based on a relevant metal *Me*. The existence ranges of temperature and composition of $MeN_{1+\delta}$, $MeCN_{\delta}$, and $Me_{1-x}Al_xCN_{\delta}$ solid solutions formed at HPHT sintering are determined. As shown, the crystal-structure features revealed in these solid solutions are in a good agreement with theoretical assumptions on the solid-phase interaction of the charge components at sintering. Thus, the accumulation of nitrogen in *Me*N and *Me*C phases is described within the atomistic diffusion model. Using the data on the excess of N in nitrides as the reference values, the main parameters of nitrogen diffusion (activation energy and rate constant) within the cBN–{TiN, HfN, VN, NbN}–Al composites are determined. The formation of Al solid solutions at cer-

Citation: N.M. Bilyavyna, V.Z. Turkevych, D.A. Stratiichuk, A.M. Kuryliuk, and O.I. Nakonechna, On the Formation of Solid Solutions at Thermobaric Sintering of PcBN Composites of cBN–*Me*N–Al and cBN–*Me*C–Al Systems, *Progress in Physics of Metals*, **25**, No. 4: 661–707 (2024)

© Publisher PH "Akademperiodyka" of the NAS of Ukraine, 2024. This is an open access article under the CC BY-ND license (https://creativecommons.org/licenses/by-nd/4.0)

tain modes of HPHT sintering is explained by the mechanism of interaction of liquid aluminium with *Me*C, which is preceded by the active formation of vacancies in the metal sublattice of these carbides. Methodologically, the x-ray diffraction study data are applied for the first time to determine the main parameters of the N-atoms' migration towards the surface of a composite at its HPHT sintering.

Keywords: cubic boron nitride (cBN), composite, mononitride, monocarbide, x-ray diffraction, crystal structure, diffusion.

1. Introduction: Retrospective Review of Superhard PcBN Materials

1.1. Cubic Boron-Nitride-Containing Ceramic Matrix Composites for Cutting Tools

The explosive development of the iron steel industry and metalworking industry continuously causes the need to create new high-strength ceramic materials for instrumental purposes from the modern materials science perspective. Traditionally, hardened steels or various cermets were used for the processing equipment. The main disadvantage of such materials is the extremely low performance of the cutting tool at high-speed processing since hardened steels were subjected to annealing under these conditions while cermets were losing their strength or experienced the increased wear of cutting edge. The use of cutting tools on the base of artificial cBN, which began to be produced conventionally in the form of micropowders and sintered ceramic products of various configurations or so-called 'superhard' materials resulted in a significant breakthrough in the processing industry. Subsequently, it was found that superhard diamond-containing composites are most effective in stone processing (especially when drilling in hard rock wells), while superhard cBN materials are effective in the metalworking industry.

The general global trend in the processing industry causes the need to increase labour productivity and forces us to look for faster methods of processing, without losing the surface roughness and quality of the product obtained. That is, taking into account the growing demand for high-speed processing and the requirements for increasing the lifecycle of the cutting tool, it is necessary to create and improve continuously novel composite materials, which would meet advanced criteria determined by the needs of the industry. Since the temperature at the point of contact between the cutting edge and the surface processed can reach 1000 °C and higher at high-speed processing, one of the ways to increase the lifecycle of the tool is the development of new ceramic materials that are more heat-resistant and more chemically inert about the surface being processed.

cBN-Al composites developed in Kyiv at the V. M. Bakul Institute for Superhard Materials of the N.A.S. of Ukraine (ISM NASU), also known as Kyborit (Киборит), are among the most commercially successful superhard materials containing cubic boron nitride. In most cases, these materi-

als replaced cermets (mainly ceramics of the WC–Co group) because of the achievement of a significant increase in the tools' lifecycle and advanced surface processing. Moreover, due to the use of Kyborit, new methods of processing the parts were developed, which previously were unavailable when using a carbide tool.

Further improvement of ceramics based on cubic boron nitride (PcBN materials) led to the creation of a wide class of new materials, so-called ceramics of the BL group, with a content of cBN up to 65 vol.% and with a binder containing a certain superhard compound. It is why these ceramics have become the most promising materials for high-speed and finishing metalworking in machine engineering and the automotive industry during hard turning of steels and cast irons. However, their efficiency at processing heat-resistant aerospace materials (*i.e.*, superalloys of Inconel 718 type) and titanium alloys is still insufficient and requires further expansion of ceramic nomenclature due to tuning the multiphase binders and variation of composition in cubic boron nitride.

The purposeful search for new binders/fillers for the cBN matrix should be based on the study of physicochemical features of the charge-components' interaction at HPHT (high pressure, high temperature) sintering, as well as on establishing the relationship between physical properties and operational characteristics of BL composite developed. It is known that both new boride and nitride phases (*Me*B_2, AlN, *etc.*) and solid solutions based on the original compounds can form BL composites as a result of reaction between initial components. Correct data on the composition of solid solutions formed at HPHT sintering can be obtained from XRD structural analysis by refining the crystal structure of each phase present in the sample synthesized under certain conditions. Here, we summarize the results of a detailed XRD study of the crystal structure of *d*-transition metal mononitrides and monocarbides, existing in the sintered at 7.7 GPa in the temperature range of 1600–2450 °C composites of cBN–*Me*N–Al (*Me*N = TiN, ZrN, HfN, VN, NbN) and cBN–*Me*C–Al in (*Me*C = TiC, ZrC, HfC, VC, NbC, TaC) systems. Analysis and systematization of the results obtained would serve as a scientific basis for the purposeful selection of promising compounds for BL material, which contains two or more *Me*N and/or *Me*C phases in addition to Al as components of the charge.

Boron nitride crystallizes into four polymorphic forms (Table 1), but just hexagonal BN (hBN) and cubic BN (cBN) are the most important and have found a wide industrial application [1, 2]. The hexagonal form is analogous to graphite and is a good lubricant, while the cubic form (with a sphalerite structure) is the second hardest material after diamond.

Hexagonal boron nitride hBN in the form of a powder is obtained by the reaction of boron oxide B_2O_3 with ammonia NH_3 at a temperature of about 2000 °C and is used as a raw material to obtain cBN by high-pressure method. cBN was first synthesized in this way by 'General Electric'

Table 1. **Selected characteristics of known cBN modifications [1, 2]**

Phase	Space group	Lattice parameter			Poisson ratio η	Density r, g/cm^3
		a, nm	c, nm	V, nm^3		
cBN	$F\bar{4}3m$	0.3615	—	0.0472	0.156	3.492
hBN	$P6_3/mmc$	0.2504	0.66612	0.0362	0.145	2.279
wBN	$P6_3mc$	0.2550	0.4230	0.0239	0.157	3.460
rBN	$R3m$	0.2504	1.004	0.0543	0.145	2.275

(U.S.A.) followed by several different approaches patented for obtaining micropowders of cubic boron nitride.

The cBN powder found its application as a free-abrasive material and as a raw material for composites of various functional purposes. Products made of superhard materials containing cBN have gained significant distribution in many industries such as machine tool construction, automobile engineering, aviation and space engineering, *etc.* The application of these PcBN materials made it possible to significantly increase the productivity and reliability of the processing tool, ensure a higher quality of the processing surface, and reduce the number of procedures, which makes the technological process more cost-effective.

1.2. PcBN Materials Classification

Due to its superior hardness, good thermal conductivity and chemical resistance (remains stable in air up to 1200 °C), polycrystalline cBN (PcBN) has been widely used in cutting tools for the machining of hard ferrous materials (hardened alloy steels, tool steels, cast iron, *etc.*) or as a reinforcing phase to enhance the hardness and wear resistance of other hard materials (*e.g.*, Al_2O_3 and WC). cBN-based products are classified as Superhard and Ultrahard in terms of hardness and, together with diamond and carbide tools, form the basis of the modern processing industry [3].

Instrumental cBN-based ceramics can be obtained at high pressures and high temperatures in three ways as presented in Fig. 1.

1.2.1. Materials with a High cBN Content (BH-Group, cBN Content Is Higher than 70 vol.%)

Cubic boron nitride can sinter independently (without activators) at high pressures and high temperatures due to plastic deformation and diffusion processes at grain boundaries, forming superhard ceramics [4–6]. Depending on the barothermal conditions of sintering, the density of the consolidated material can reach 98%. Superhard ceramics of the cBN–Al system, in which the mass fraction of cubic boron nitride reaches about 90–96% is one of such dense PcBN materials. Such composite was designed and obtained by reaction sintering of cBN micropowders (from 10 μm to 40 μm

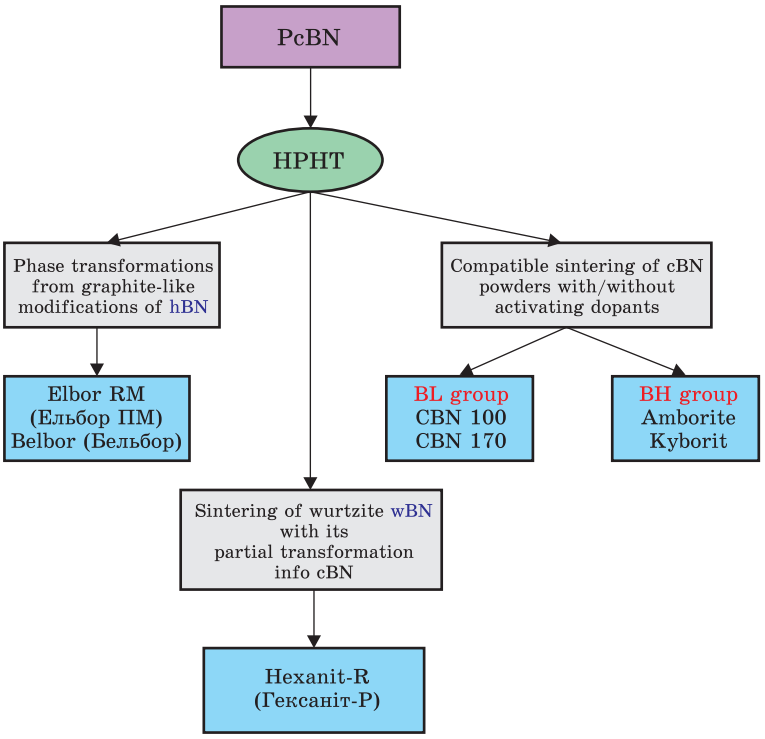

Fig. 1. Schematic representation of PcBN materials manufacturing

of grain size) together with aluminium powder in high-pressure apparatus (pressure is up to 5 GPa) at ISM NASU. In the process of HPHT sintering, the solid-state reaction between boron nitride and aluminium leads to the formation of a small amount of aluminium borides (AlB_2, AlB_{12}), AlN and Al_2O_3 (result of aluminium with residual oxygen interaction) [7–10]. Today, this material is produced under the trademark Kyborit (Ukrainian patents Nos. 25281A and 28827A). The main physical and technical characteristics of Kyborit material are as follow: density (ρ) is of 3.40 g/cm^3, Young's modulus (E) is of 880 GPa, shear modulus (G) is of 372 GPa, compression modulus (B) is of 450 GPa, Poisson's ratio (η) is of 0.160, hardness ($HK10$) is of 32–36 GPa, fracture toughness (K_{1C}) is of 10–13.5 MPa$\cdot$m$^{1/2}$. Kyborit is effectively applicable for the turning of hardened steels and wear-resistant alloys; it is also used as an anvil of the second stage in high-pressure multiple-blanking tools.

One more important design of ceramic cutting plates of ISM NASU is patented as Borsynit (Борсиніт) (Ukrainian patent No. 70820A) and also belongs to PcBN materials with a high content of cubic boron nitride (BH-group) [11, 12]. This ultrahard composite contains 90–95% cBN (average grain size of 5–10 μm) and heat-resistant additive Si_3N_4, which is evenly placed between cBN grains without forming a continuous framework. The

main physical and technical characteristics of Borsynit material are: ρ is of 3.45 g/cm^3, E is of 860 GPa, G is of 366 GPa, B is of 440 GPa, η is of 0.175, $HK10$ is of 36–39 GPa, K_{1C} is of 11.7 MPa·m$^{1/2}$. Instrument material Borsynit is successfully applicable for finishing treatment and processing of hardened carbon and alloy steels, high-strength and wear-resistant cast irons, heat-resistant chrome–nickel alloys as well as for the processing of WC–Co cermets (>15%).

One of the known international analogues of BH-group materials is the KBN900 composite designed and developed by Kyocera (Kyoto, Japan). KBN900 consists of a cBN ceramic matrix, in which aluminium phases are evenly distributed. According to its characteristics, KBN 900 material is not inferior to Borsynit and Kyborit and is successfully applied for finishing and rough metalworking.

Generally, materials of the BH group with metal or ceramic additives such as Ni, Co, AlB_2 or AlN are usually applied for rough and intermittent machining of steels and cast irons [13].

1.2.2. Materials with a Low cBN Content (BL-Group, cBN Content Varies from 40 to 60 vol.%)

It is known that the local temperature in the cutting zone can exceed 1000 °C, which leads to the activation of chemical interaction between the tool and processed part, and contributes to the oxidation of the contact zone with air oxygen. These processes affect the wear of the cutting tool, the degradation geometry of the cutting edge, and the reduction of quality and precision of surface processing [14–17]. To some extent, these defects can be prevented by adding heat-resistant and oxidation-resistant compounds to cBN-based ceramics based on. That is why materials of the BL group with a high content (up to 60 vol.%) of refractory ceramic phases are usually used in continuous processing due to their high chemical resistance [18–20].

In other words, the high thermal and chemical stability of BL group materials is provided by the matrix of cBN grains, while their physical and mechanical properties can be tuned by adding to this matrix a certain filler material (binder), which contains refractory ceramic superhard phases, the influence of which on the operational characteristics of cutting inserts can be decisive. Titanium compounds (TiC, TiN and Ti(C,N)) are widely used as binders for the cBN matrix [21–23]. Meanwhile, the authors of this article are working on expanding the range of binders and approaches to design the advanced composition of cutting tools. Recently, new compositions of binders with carbides or nitrides of some refractory metals (*i.e.*, Cr, V, Ta, Zr, *etc.*) in combination with aluminium have been designed and optimized [24–33].

Materials of the BL group with binders of refractory compounds are applied for high-speed finishing of heat-resistant aerospace materials (for example, superalloys of the Inconel 718 type, AISI 4340, Caldie) and titanium alloys.

1.3. Composites of BL-Group of cBN–MeN–Al and cBN–MeC–Al Systems

Mononitrides and monocarbides of transition metals with NaCl-type crystal structures are characterized by high melting points and hardness and are usually resistant to oxidation (Table 2), which makes them attractive for application as binders for cubic boron nitride-based composites.

Numerous studies [29–43] of composites of cBN–*Me*N–Al and cBN–*Me*C–Al systems (where *Me* = Ti, Zr, Hf, V, Nb, Ta; the volume ratio of charge components is 60:35:5) were provided at V. M. Bakul Institute for Superhard Materials, National Academy of Science of Ukraine (Kyiv) by HPHT sintering (pressure 7.7 GPa, temperature 1600–2450 °C). It should be noted that the physical and chemical properties, and operational characteristics of these composites (Table 3) were studied in detail by a set of suitable methods [33–43], resulting in a large amount of experimental material collected. Analysis and systematization of the results obtained could provide useful information on the interaction of charge components at barothermal sintering.

Results of XRD studies of the compacts obtained have shown that barothermal treatment results in the formation of reaction products of the charge components in sintered samples (usually MeB_2 and AlN), as well as their oxidation products (ZrO_2 and Al_2O_3) already at 1750 °C (cBN–*Me*N–

Table 2. **Selected characteristics and main thermodynamic parameters of *d*-transition metal mononitrides and monocarbides with NaCl-type structure**

Phase	Lattice parameter* *a*, nm	Hardness *H*, GPa	Melting temperature *T*, °C	Formation enthalpy ΔH^0_{298}, kJ/mol	Entropy S^0_{298}, J/(mol·K)	Dissociation energy D_0, kJ/mol
*Me*N mononitrides						
TiN	0.4240	20	2930	−323	30	1261
ZrN	0.4575	16	2980	−372	38	1437
HfN	0.4526	22	2982–3310	−374	45	1461
VN	0.4130	?	2050	−298	37	1197
NbN	0.4390	14	2573	−234	33	1420
TaN	0.4360	18	3090	−252	42	1505
cBN	0.3615	up to 114	2973	−476	7	942 ?
hBN	—	—	3000	−250	14	1277
*Me*C monocarbides						
TiC	0.4332	32	3260	−82.52	25	1388
ZrC	0.4697	30	2532	−97	33	1508
HfC	0.4637	28	3900	−102.4	40	1537
VC	0.4173	25	2810	−57.8	30	?
NbC	0.4470	22	3490	−66.8	35	1563
TaC	0.4455	17	3880	−68.4	42	1637
Ti(C, N) carbonitride						
Ti(C,N)	0.4282	27	—	—	—	—

* Lattice parameters of nitrides and carbides in a charge processed in a ball mill.

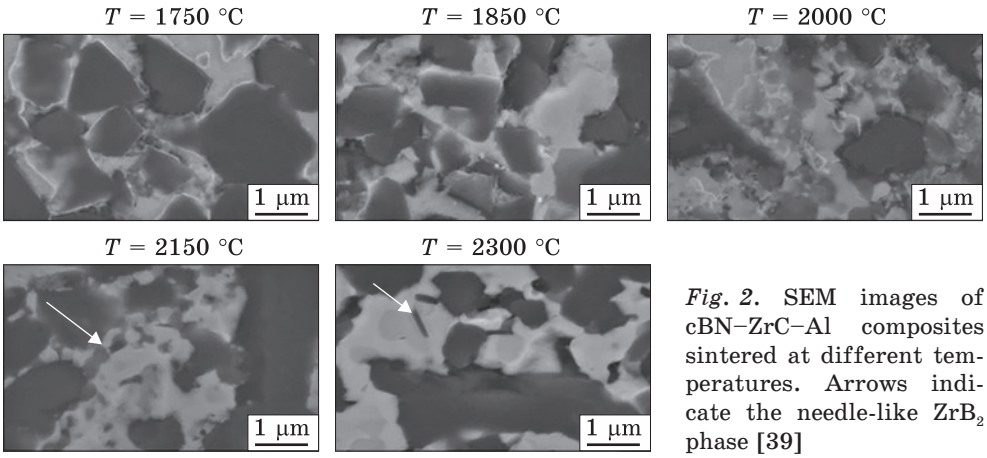

Fig. 2. SEM images of cBN–ZrC–Al composites sintered at different temperatures. Arrows indicate the needle-like ZrB_2 phase [39]

Table 3. **Main functional characteristics of cBN–*Me*N–Al and cBN–*Me*C–Al composites HPHT sintered at 2150 °C**

Composite	Young's modulus E, GPa	Shear modulus G, GPa	Hardness HV_{50}, GPa	Fracture toughness K_{1C}, MPa·m$^{1/2}$
cBN–*Me*N–Al system				
cBN–TiN–Al	600	272	32	5.6
cBN–ZrN–Al	510	220	23	6.0
cBN–HfN–Al	467	183	31	5.0
cBN–VN–Al	550	223	31	4.9
cBN–NbN–Al	499	205	29	4.8
cBN–*Me*C–Al system				
cBN–TiC–Al	630	—	43	6.5
cBN–ZrC–Al	502	225	31	6.0
cBN–HfC–Al	570	—	27	6.5
cBN–VC–Al	625	253	37	7.0
cBN–NbC–Al	602	246	36	6.2
cBN–TaC–Al	542	212	34	5.4

Al systems) or above 2000 °C (cBN–*Me*C–Al systems). According to quantitative phase analysis, the content of these phases almost does not change with the sintering temperature increasing. It is also shown that the refined values of lattice parameters of borides MeB_2 and AlN in sintering products either completely correspond to the reference data or are very close to them. However, the lattice parameters of TiN, ZrN, HfN, VN, NbN mononitrides and TiC, ZrC, HfC, VC, NbC, TaC monocarbides vary with increasing temperature of HPHT sintering and differ significantly from initial-phases' values [33–43]. This may indicate the formation of solid solutions based on the specified nitrides or carbides.

One of the methods, which allow us to confirm or decline the fact of solid solution formation and determine its elemental composition, is EDS analysis. However, as it was shown, the fine crystalline products of the reaction interaction of the charge components (MeB_2, AlN, oxides) in compacts studied are usually located along the grain boundaries of the main phases cBN, *Me*N, *Me*C (white shell on ZrC and cBN grains in Fig. 2) and their presence shields the grains of the main phases during elemental composition studies, and EDS analysis provides localized studies. In addition, N, B or Al components, which can be dissolved in carbides or nitrides, have a very small scattering power compared to *d*-metals, forming the framework of *Me*N and *Me*C phases.

Thus, EDS studies of the HPHT sintering products do not provide reliable data on forming solid solutions based on mononitrides or monocarbides of transition metals and their elemental composition.

1.4. Research Statement

As reported in Refs. [33–43], a comprehensive XRD and STEM study of BL composites of cBN–*Me*N–Al and cBN–*Me*C–Al systems HPHT sintered at 7.7 GPa in a wide temperature range (1600–2450 °C) have revealed the formation of solid solutions based on nitrides or carbides counterparts. However, quantitative characteristics regarding the content of additional components in *Me*N and *Me*C were not present in these works.

It is known that to obtain additional information on the materials' crystal structure such as the transformation of separate crystal phases during sintering the procedure of crystal structure refinement needs to be applied since an ordinary XRD study provides information just on phase composition and lattice parameters.

It should also be noted that the fundamental difference between EDS and XRD methods is that EDS analysis detects a signal from a separate, small sample surface (∅ up to 100 nm), while XRD analysis processes the signal (diffraction pattern) obtained from the sample surface ∅ up to 15 mm. That is EDS analysis provides information on the composition of a *local* area on the surface, while XRD collects integral data on the structure and composition of a separate phase. Both methods certainly complement each other and together can provide reliable information about the state and composition of the phases studied.

Here, data on the formation of solid solutions based on mononitrides or monocarbides of transition *d*-metals in the products of HPHT sintering of cBN–*Me*N–Al and cBN–*Me*C–Al systems were obtained by XRD structural analysis with crystal structure refinement of each phase existing in the samples synthesized under certain sintering conditions. Analysis of the information obtained by this method makes it possible:

• to determine whether the crystal structure of the resulting solid solution belongs to the original structural type of NaCl or its formation is accompanied by a modification of this structure;

• to follow the dependence of solid solution composition on temperature regimes of HPHT sintering;

• to identify a possible correlation between the operational characteristics of composites manufactured and the presence of solid solutions of a certain composition in them.

In general, such analysis, based on the results of the study of simple cBN–*Me*N–Al and cBN–*Me*C–Al system composites will serve as a scientific background for the purposeful selection of promising binders for PcBN materials, which contain two or more *Me*N/*Me*C phase in addition to aluminium as components of the initial charge.

2. Materials and Methods

2.1. Materials and Samples Preparation

Samples of PcBN composites were synthesized from commercial micropowders (grain size up to 15 μm) of cBN (Element Six LLC), powders of *d*-transition metals *Me*N and *Me*C (Onyxmet), as well as Al flakes (ABCR GmbH) at ISM NASU. Initial charge with the same volume ratio of components cBN : *Me*N : Al (*Me* = Ti, Zr, Hf, V, Nb) or cBN:*Me*C:Al (*Me* = Ti, Zr, Hf, V, Nb, Ta) as 60 : 35 : 5 was grinded to a size of 1–5 μm and mixed in a Pulverisette 6 planetary mill (Fritsch GmbH) in isopropyl alcohol. Homogenized mixture was further compacted in steel moulds. Sintering of the compressed charge was carried out in a high-pressure apparatus of 'Toroid-30' type at 7.7 GPa in the temperature range of 1600–2450 °C using graphite heaters with isothermal holding at a given temperature for 45 s. It should also be noted that a series of samples (up to 7 composites) was manufactured at a constant set of sintering temperatures for each cBN–*Me*N–Al and cBN–*Me*C–Al system.

2.2. Experimental Methods

Diffraction patterns of the composites synthesised were obtained by STOE STADI MP XRD apparatus using CuK_α filtered radiation, the angular interval of shooting was 10–100°, scanning step was 0.015°, and exposure time at each point was 3 s. For primary processing of XRD data, for qualitative and quantitative phase analysis, and structural calculations, we used the original software package [44] developed at Taras Shevchenko National University of Kyiv, which contains a full set of Rietveld procedures.

More specifically, the primary processing of XRD data was provided by full-profile analysis, interpolating the experimental diffraction peak with analytical Lorentzian function, which determines the gravity centres of $K_{\alpha 1}$ peaks (with accuracies of ±(0.001–0.01)° and, for their integral intensities, of ±(5–10)%). Parameters of the crystal lattice of each phase component, for which identification was carried out during the phase analysis, were refined by the method of the least squares simultaneously

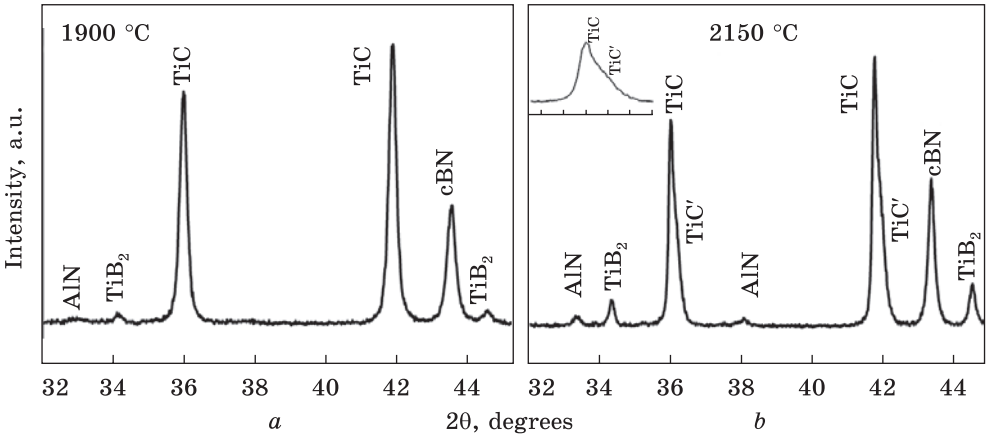

Fig. 3. Fragments of diffraction patterns cBN–TiC–Al composite sintered at different temperatures [57]

with the analytical refinement of the alignment accuracy of the sample's working surface on the diffractometer. The relative error in determining the parameters of the crystal lattice does not exceed 0.02%. Verification of the crystal structure models proposed followed by the refinement of their co-ordinate and thermal parameters by the least squares method as well as the occupation factors of corresponding regular point systems, was carried out using a set of programs for structural calculations. The correctness of the model proposed after its refinement was checked in graphic mode and evaluated by the coincidence of the intensities of diffraction reflections (experimental and calculated according to this model), as well as by the value of the Bragg reliability factor R_B, which was usually $R_B < 0.02$. As an example, Fig. 3 presents fragments of typical diffraction patterns of the composite studied.

3. Impact of HPHT Sintering on the Crystal Structure of Mononitrides and Monocarbides of *d*-Transition Metals

3.1. MeN Crystal Structure of PcBN Composites

3.1.1. XRD Study of MeN Phases

According to the XRD phase analysis, barothermal treatment of initial mixtures of cBN–*Me*N–Al (60 : 35 : 5) (*Me* = Ti, Zr, Hf, V, Nb) at sintering temperatures higher than 1800 °C leads to the formation of the following phases: MeB_2/NbB, AlN, ZrO_2 and α-Al_2O_3 (Table 4). The refined values of crystal lattice parameters of TiN, ZrN, HfN, VN, and NbN mononitrides are changed significantly with the sintering temperature increase (Table 4). To follow the impact of sintering conditions on the experimental temperature dependences of lattice parameters $a(T)$, the lattice distortions ε were

estimated. To compare the experimental temperature dependences of lattice parameters $a(T)$, the nature of change in distortions of those lattices at sintering conditions was considered. The lattice distortion was calculated as $\varepsilon = 100\% \times (a_T - a_{20})/a_T$, where a_T is the lattice parameter at a certain sintering temperature T; a_{20} is the lattice parameter of the initial mixture (Table 2). The values calculated are plotted in Fig. 4.

A detailed study of the crystal structure of phases, existing in samples synthesized was provided to establish the factors that lead to changes in the lattice parameters of *Me*N. It should also be noted that using Ta–Al mixture as a binder results in the formation of TaN phase with different from NaCl-type crystal structure modification in HPHT sintered PcBN composites. Therefore, we do not consider this compound in the present study.

Table 4. **The phase composition of cBN–*Me*N–Al composites HPHT sintered at 7.7 GPa**

Sintering temperature T, °C	Phase composition	Lattice parameter a, nm
		Composites of
1750	cBN(60)[1] + TiN(33) + TiB_2(3) + AlN(4)	0.42498
1850	cBN(60) + TiN(33) + TiB_2(3) + AlN(4)	0.42452
2000	cBN(61) + TiN(33) + TiB_2(2) + AlN(4)	0.42440
2150	cBN(60) + TiN(34) + TiB_2(2) + AlN(4)	0.42429
2300	cBN(60) + TiN(33) + TiB_2(3) + AlN(4)	0.42428
		Composites of
1750	cBN(62)[1] + ZrN(34) + ZrO_2(4)	0.42498
1900	cBN(61) + ZrN(32) + ZrB_2(3) + ZrO_2(4)	0.42452
2000	cBN(60) + ZrN(29) + ZrB_2(3) + ZrO_2(3) + α-Al_2O_3(5)	0.42440
2150	cBN(60) + ZrN(29) + ZrB_2(3) + ZrO_2(3) + α-Al_2O_3(5)	0.42429
2300	cBN(60) + ZrN(29) + ZrB_2(3) + ZrO_2(3) + α-Al_2O_3(5)	0.42428
		Composites of
1900	cBN(63)[1] + HfN(30) + HfB_2(3) + HfN′(4)	0.4541[2]
2000	cBN(61) + HfN(31) + HfB_2(3) + HfN′(5)	0.4544
2150	cBN(60) + HfN(31) + HfB_2(3)	0.4542
2300	cBN(61) + HfN″(31) + HfB_2(3) + HfN(5)	0.45833[3]
2450	cBN(63) + HfN″(30) + HfB_2(3) + HfN(4)	0.45872
		Composites of
1600	cBN(63)[1] + VN(37)	0.4131
1750	cBN(63) + VN(37)	0.4133
1900	cBN(62) + VN(36)+α-Al_2O_3 · (2)	0.41319
2000	cBN(62) + VN(36) + α-Al_2O_3 · (2)	0.41311
2150	cBN(62) + VN(36) + α-Al_2O_3 · (2)	0.41301
2300	cBN(62) + VN(36) + α-Al_2O_3 · (2)	0.41296

[1] In parentheses, the content of phases is given in vol.%; [2] *Me*N is characterized below; in relation to corresponding values in the charge; [5] 4*a* position is completely occupied by

Crystal-structure calculations of *Me*N phases existing in the charge processed in a ball mill were carried out in the model of structural NaCl type. As a result, it was shown that the crystal structure of these phases is defective with a composition of $MeN_{0.95}$, as is usually observed for these phases. Crystal structures of *Me*N, existing in HPHT sintered samples were also calculated in the model of NaCl structural type. However, the obtained results indicated that, when the 4*a* position is completely occupied with *d*-metal atoms, the occupation of the 4*b* position with nitrogen atoms is >> 1. It seems like more than 4 nitrogen atoms are placed in this position, which is unacceptable from the point of view of XRD structural analysis. This is the reason why slightly different structural models were proposed and tested for nitrides of HPHT sintering products.

and crystal structure characteristics of their *Me*N phases

Lattice distortion ε, %[4]	Number of N atoms[5]			N content, at.%	
	4*b* position	24*e* position	Total number of atoms	Total	Excess nitrogen δ
cBN–TiN–Al system					
0.23113	2.93	3.18	6.11	60.43	12.43
0.12264	2.54	2.9	5.44	57.63	9.63
0.09434	2.46	2.55	5.01	55.60	7.60
0.06840	2.38	2.31	4.69	53.97	5.97
0.06604	2.33	2.29	4.62	53.60	5.60
cBN–ZrN–Al system					
0.02623	3.71	0.25	3.96	49.75	1.75
0.05027	3.53	1.02	4.55	53.22	5.22
0.03497	3.44	1.24	4.68	53.92	5.92
0.02404	3.31	1.72	5.03	55.70	7.70
0.01093	3.37	1.82	5.19	56.47	8.47
cBN–HfN–Al system					
0.34026	1.81	5.98	7.79	66.07	18.07
0.40654	2.25	4.86	7.11	64.00	16.00
0.34909	3.81	1.09	4.9	55.06	7.07
1.26602	3.52	1.82	5.34	57.17	9.16
1.34998	4.00	5.31	9.31	69.95	21.95
cBN–VN–Al system					
0.01937	3.71	1.84	5.55	58.11	10.11
0.07264	3.68	1.35	5.03	55.70	7.70
0.04600	3.66	1.1	4.76	54.34	6.34
0.02663	3.66	0.7	4.36	52.15	4.15
0.00242	3.68	0.64	4.32	51.92	3.92
–0.00969	3.68	0.37	4.05	50.31	2.31

[3] *Me*N′ is characterized below; [4] Lattice deformation of nitrides in composites is estimated corresponding *Me* atoms (contains 4 atoms)

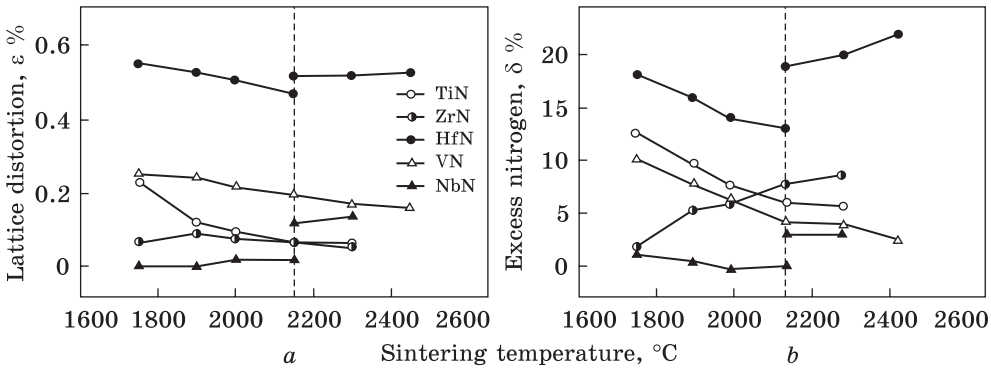

Fig. 4. **Fig. 4.** Temperature dependences of the crystal lattice distortion ε of *Me*N phase of cBN–*Me*N–Al composites at HPHT sintering (*a*) and excess nitrogen in them δ (*b*)

Calculation of several placement options for all nitrogen atoms in the *Me*N structure finally led to a model in which additional nitrogen atoms N(2) are placed in the 24*e* position, forming an octahedron with a centre occupied or rather not occupied by N(1) atoms of the main 4*b* position. That is, *Me*N composites are characterized by the following arrangement of atoms according to the regular point systems of *Fm*3*m* (No. 225):

$4q_1 Me$ are placed in 4*a* (0 0 0);

$4q_2$N(1) are placed in 4*b* (0.5 0.5 0.5);

$24q_3$N(2) are placed in 24*e* (*x* 0 0),

where q_1, q_2, and q_3 are the occupation factors of metal and nitrogen atoms of positions ($q \leq 1$), *x* co-ordinate takes the value of ≈0.32 or ≈0.28 depending on the nitride type. As an example, the results of the crystal structure refinement of TiN existing in the initial charge and one of the sintered samples are listed in Table 5.

Table 5 presents a model of the modified NaCl crystal structure for *Me*N phases of HPHT sintering products. This model was developed and described in detail in our papers [45, 46].

According to the results of structural calculations, Al atoms do not participate in the formation of *Me*N structure. Obviously, that is why they actively interact with residual oxygen and nitrogen, forming α-Al_2O_3 and AlN phases (Table 4).

Calculations performed demonstrate that the modified NaCl-type structure described above (Table 5) is typical for each of the mononitrides of cBN–*Me*N–Al charge subjected to HPHT sintering. Refined within this model structural data are listed in Table 4 for TiN, ZrN, HfN, VN, or NbN. More specifically, these are the data on the number of nitrogen atoms in 4*b* and 24*e* positions (main and additional) and the refined full nitrogen content in nitrides (*i.e.*, their composition). The

reliability factor R_B of this model does not exceed 0.011 that indicates its correctness.

Summarizing all the above, metal atoms of *Me*N phases completely occupy the 4*a* position, which corresponds to 4 atoms per unit cell, while 4*b* and 24*e* positions are somehow defective (Table 4). The pattern of possible placement of N(2) atoms around one of four possible defective 4*b* positions with the coordinate of (0 0.5 0) is illustrated in Fig. 5.

We should note that analysis of interatomic distances in the structures of *Me*N phase shows that the smallest observed distance N(1)–N(2) for nitrogen atoms is approximately 0.76 nm, while the distances N(2)–N(2) (octahedron edge length formed by N(2) atoms as illustrated in Fig. 5) are 1.086 nm, and this value is very close to the bond length between N atoms in the diatomic molecule of N_2 gas (1.09 nm).

3.1.2. Origin of the Interaction of MeN Phase with Lattice-Migrating Nitrogen

Obtained XRD data has revealed the presence of MeB_2 and sometimes AlN phases in products of HPHT sintering of cBN–*Me*N–Al charge. For example, TiB_2 and AlN in cBN–TiN–Al system are located at the contact

Table 5. **TiN crystal structure calculations**

TiN of initial charge (NaCl type structure)					
Atom	Position	Occupation	*X*	*Y*	Z
Ti	4*a*	1.000(1)	0	0	0
N	4*b*	0.936(3)	0.5	0.5	0.5
Space group			*Fm*3*m* (No. 225)		
Lattice parameter *a*, nm			0.42395(2)		
Temperature coefficient *B*, nm^2			$1.19(7)\cdot10^{-2}$		
Phase composition calculated, at.%			51.5Ti + 48.5N		
Reliability factor, R_B			0.013		
TiN of sintered at 7.7 GPa and 2000 °C composite (modified NaCl type structure)					
Atom	Position	Occupation	*X*	*Y*	Z
Ti	4*a*	1.000(1)	0	0	0
N(1)	4*b*	0.607(3)	0.5	0.5	0.5
N(2)	24*e*	0.097(3)	0.320	0	0
Space group			*Fm*3*m* (No. 225)		
Lattice parameter *a*, nm			0.42440(9)		
Temperature coefficient *B*, nm^2			$0.80(1)\cdot10^{-2}$		
Phase composition calculated, at.%			45.7Ti + 54.3N		
Reliability factor R_B			0.008		

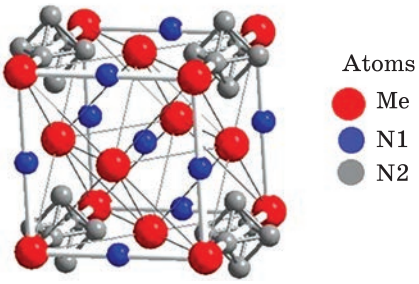

Fig. 5. Atoms arrangement in the crystal structure of *Me*N, existing in HPHT sintered cBN–*Me*N–Al composites

boundaries of cBN and TiN grains according to electron microscopy data (white chains in Fig. 6); TiN itself undergoes certain structural transformations on the report of XRD analysis.

To sum up:

(i) *Me* atoms occupy their position completely ($q_1 = 1$);

(ii) N atoms are located at two defective positions ($q_2 < 1$, $q_3 << 1$);

(iii) the value of the co-ordinate parameter x depends on the type of metal that forms *Me*N;

(iv) Al and B atoms do not participate in the formation of *Me*N crystal structure.

Considering these features, the composition of each *Me*N phase was determined by joint refinement of occupation factors of q_2 and q_3 position. Excess nitrogen (δ) present in *Me*N phase was calculated in relation to the nitrogen content in a charge (49 at.%). Fig. 4, *b* illustrates the behaviour of δ parameter in dependence on sintering temperature, and Fig. 7 clearly shows that it is the excess of nitrogen that leads to the distortion of nitride-crystal lattice. Specific case of ZrN should also be noted (Figs. 4, *b* and 7), where an increase in the sintering temperature is accompanied by an increase in δ while keeping relatively small lattice distortion (Table 4). Besides, an active process of penetration of smaller oxygen atoms into ZrN crystal lattice is also observed, as we discovered previously for ZrC carbide [47]. Therefore, the excess nitrogen obtained from XRD data is actually the total content of nitrogen and oxygen that penetrated ZrN lattice at high sintering temperatures.

It is important to keep in mind that x-ray radiation provides the diffraction pattern from a certain surface layer of the sample studied (< 0.01 mm). Therefore, the analysed features of *Me*N crystal structure correspond to the surface phenomena. Formation of such nitrogen-enriched layer on the surface of compact samples or films of transition metals nitrides was previously reported in Refs. [31, 48–50]. Obviously, the existing nitrogen enrichment of surface nitrides occurs due to its transition from the internal regions of sample, *i.e.*, due to diffusion processes.

D. G. Sangiovanni *et al.* [51] studied the diffusion of point interstitial defects (migrating nitrogen atoms and lattice vacancies) in TiN by molecular dynamics simulations (AIMD and CMD). They described an atomistic process that controls the spontaneous formation of pairs from interstitial N^I nitrogen atoms and N^V crystal lattice vacancies (so-called Frenkel pairs), which can form even in defect-free TiN. This means that the N atom of one lattice leaves its usual position and connects with the N atom

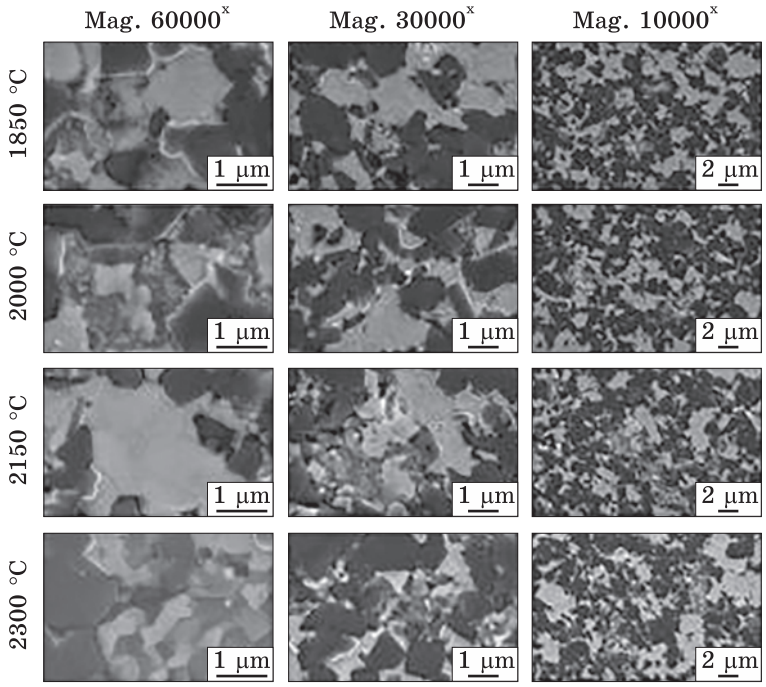

Fig. 6. SEM images of cBN–TiN–Al composites sintered at different temperatures [34]

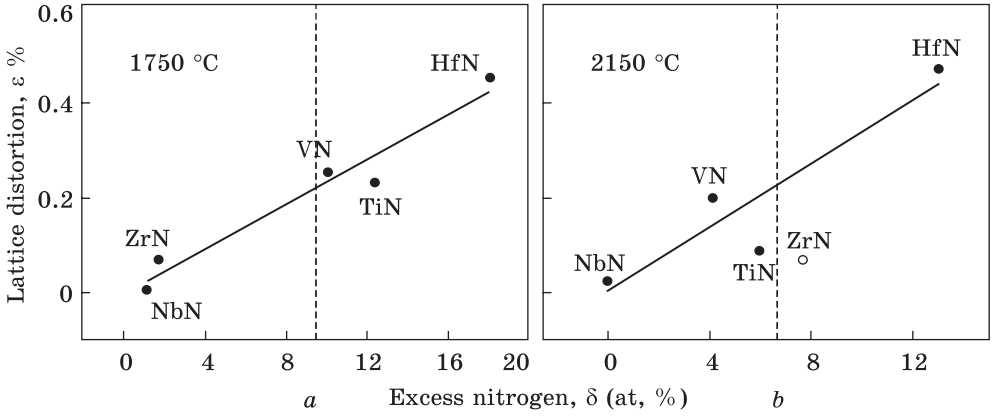

Fig. 7. *Me*N crystal lattice distortion in relation to excess nitrogen for HPHT sintered cBN–*Me*N–Al composites

of the neighbouring lattice. According to Ref. [51], about 50% of these processes also lead to the exchange of two nitrogen atoms. Sometimes, the migrating interstitial nitrogen atom can contribute to the formation of a Frenkel pair, tearing out the existing lattice anion with the formation of a new vacancy. Comparing the experimental results presented in this paper

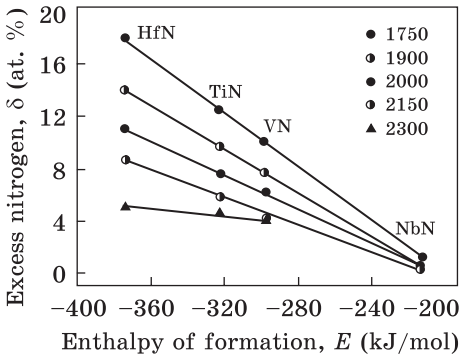

Fig. 8. Excess nitrogen accumulated by *Me*N crystal lattice at certain sintering temperatur

on the crystal structure of *Me*N (Table 5) and theoretical models of Refs. [48,51], describing the diffusion of nitrogen atoms, one can conclude that it is the statistical placement of nitrogen atoms along the vertices of octahedra (N^I atoms in 24*e* position) around existing vacancy in 4*b* position (N^V) (Fig. 5) is responsible for the formation of N^I–N^V Frenkel pairs. Moreover, if two Frenkel pairs are formed around such vacancy, then the neighbouring internodal N^I–N^I atoms form a bond, imitating a diatomic N_2 molecule. That is, the barothermal load conditions initiate diffusion flows of nitrogen atoms (decomposition products of *Me*N and cBN), tending to the surface of the composite because of the temperature gradient in the reaction zone. In turn, this determines the surface saturation with nitrogen (Table 4, Fig. 4, *b*).

Analysis of XRD data also revealed that the excess of nitrogen accumulated by *Me*N on the surface of composites at HPHT sintering of the charge (Table 4) correlates with the enthalpy of formation of these nitrides (Fig. 8). Namely, the content of excess nitrogen decreases linearly in the series of HfN → TiN → VN → NbN (prone to oxidation ZrN is not considered). That is, the HfN phase captures most of the nitrogen that goes to the sample surface to leave it as N_2 gas. Moreover, the N_2 molecule is previously formed in the crystal structure of the nitride itself from N(2) atoms located at the adjacent vertices of the octahedron at interatomic distances of ≈0.11 nm (Fig. 5). It should also be noted that the process of nitrogen accumulation in *Me*N is inhibited due to intensification of the formation of free N_2 molecules at sintering temperatures higher than 2150 °C (Fig. 8).

In our opinion, the excess of nitrogen in *Me*N calculated from XRD data (Table 4) can serve as a reference value for determining the parameters of the nitrogen atoms migration process from the bulk to the surface of the sample. It is known that diffusion, like most simple processes in a solid state (oxidation, chemical reactions, *etc.*), is well described by the Arrhenius equation:

$$D = D_0 \exp\left(E_a/(RT)\right), \qquad (1)$$

where D is the diffusion coefficient, D_0 is the temperature independent factor, R is the universal gas constant (R = 8.3145 J/(mol · K^{-1})), E_a is the activation energy of diffusion [J/mol], T is the temperature of HPHT sintering [K].

Assuming that the amount of nitrogen following to the sample surface from the reaction zone during 1 s of samples' exposure at HPHT processing is proportional to $C_N/45$ (where C_N is nitrogen content in moles, 45 [s] is the sintering time), then this value can be considered as a certain analogue of D ($C_N/45$ μ D) with the accuracy factor that describes the area of diffusion flow. Following Eq. (1), the activation energy of nitrogen atoms migration from bulk of the composite to its surface can be determined from the graphs plotted in the co-ordinates ln(D) *vs*. 1/(RT). These plots are linear in the temperature range of 1750–2150 °C for TiN, HfN, VN and NbN; so, we can determine the activation energy of nitrogen migration (Table 6, Fig. 9). Calculated values obtained are quite reasonable, since the activation energy of nitrogen diffusion is usually 0.15 and 0.75 eV for dislocation and bulk mechanisms, respectively.

It should be noted that when calculating the parameters of diffusion (Table 6), only nitrogen captured by surface nitrides was taken into account. In our opinion, almost the same slope of δ(E) plots in Fig. 9 for 1750, 1900, 2000 and 2150 °C allow us to assume that the release of nitrogen as N_2 gas is insignificant at these sintering temperatures, and the intensive release of nitrogen starts only at temperatures higher than 2150 °C (δ(E) slope changes significantly at 2300 °C).

Likely, *Me*N phases together with cBN act as a source of additional nitriding of the sample surface at HPHT sintering. Such nitrogen enrichment of the surface of cBN–*Me*N–Al composites should have a positive effect on some of its surface properties such as nanohardness, wear resistance, and corrosion resistance. H. Xie *et al.* [31], studying the composite of the cBN–TiN system, showed that the average microhardness on its surface is somewhat higher than in the bulk, namely, these values are 33.23 and 32.24 GPa for the sample studied, respectively.

XRD and electron microscopic studies showed [37, 38] that the phase composition of HPHT sintered composites of cBN–TiN–Al and cBN–VN–Al systems and their microstructure (on the surface), as well as density (throughout the volume) are almost unchanged in the temperature range

Table 6. **Nitrogen migration in HPHT sintered cBN–{TiN, HfN, VN, NbN}–Al composites**

Nitride	Formation enthalpy E, kJ/mol	Activation energy of diffusion Q, kJ/mol	Activation energy of diffusion* Q, eV	Diffusion coefficient** D_0, mol/c
HfN	–374	33.5	0.347	5.25×10^{-2}
TiN	–323	72.9	0.756	3.36×10^{-3}
VN	–298	85.7	0.888	1.27×10^{-3}
NbN	–213	168.9	1.750	8.00×10^{-7}

* Activation energy of diffusion calculated per individual nitrogen atom. ** Diffusion coefficient corresponds to the migration rate of N atoms

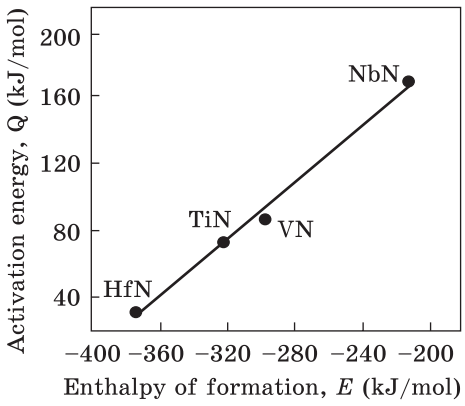

Fig. 9. Dependence of the activation energy of nitrogen diffusion in *Me*N at HPHT sintering of cBN–{TiN, HfN, VN, NbN}–Al composites on the enthalpy of their formation

of 1750–2300 °C. However, the main macrocharacteristics of composites, such as hardness, the Young's modulus, shear modulus, and fracture toughness slightly vary in this sintering temperature range. Taking into account that the temperature dependences of crystal lattice parameters of TiN and VN, and the excess of nitrogen for these systems have the same character (Fig. 4), the dependence of the above-mentioned macrocharacteristics on the amount of excess nitrogen determined by XRD in TiN and VN nitrides was considered for the composites of cBN–{TiN, VN}–Al systems (Table 4). Therefore, we followed the changes of mentioned parameters in dependence on a characteristic that varies significantly with sintering temperature increasing. For comparison, Young's modulus dependences of composites of cBN–{TiN, VN}–Al systems are plotted in two co-ordinate systems, namely, an increase of the sintering temperature and a decrease of the nitrogen excess (Fig. 10). At the same time, it should be noted that since the excess of nitrogen in nitrides changes monotonically with sintering temperature (Fig. 4), graphs like Fig. 10 have illustrative nature.

Enrichment by nitrogen of *Me*N surface nitrides automatically leads to depletion of the bulk regions of composites with nitrogen, which probably affects such volumetric characteristics of the material as Vickers hardness, Young's modulus, shear modulus, and fracture toughness. S. Yu *et al.* [52] have modelled from the first principles the impact of nitrogen content on TiN mechanical properties. They have shown [52] that at normal pressure, a conditional decrease of nitrogen in TiN from 50 to 40 at.% results in an essential decrease of mechanical characteristics: Young's modulus changes from 533 to 347 GPa, hardness decreases from 24 to 16 GPa, and shear modulus changes from 215 to 138 GPa (the relative change of these values is about 30%). For HPHT sintered composites of the cBN–{TiN, VN}–Al systems the experimental meanings of these values also gradually decrease with nitrogen depletion of the sample volume, but their relative change does not exceed 15% [37, 38].

It should also be noted that the authors of Ref. [52] theoretically predict that TiN_2 phase can be stable at high pressure (60 GPa) due to its existence in the structure of so-called encapsulated N_2 dumbbells with the interatomic distance of ≈0.13 nm. Such N_2 dumbbells form in the model of

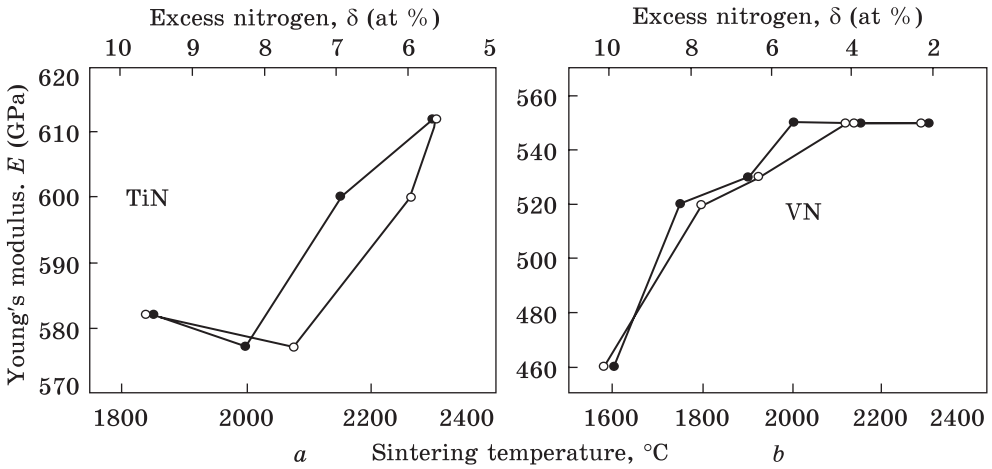

Fig. 10. Dependences of the Young's modulus on sintering temperature (black circles) [37, 38] and on the excess nitrogen (white circles) in the nitrides of cBN–TiN–Al (*a*) and cBN–VN–Al (*b*) systems

the modified NaCl-type structure proposed here for nitrogen-rich *Me*N (Table 5, Fig. 5).

For the composites of the systems described above, the diffusion mechanism is based on the movement of nitrogen atoms through vacancies and internodes of crystal lattices of nitrides. That is why D_0 is a coefficient that is directly related to the structure of the nitride (time of settled life of a diffusing atom; path of free movement, *etc.*). As a result of the calculations, it is shown that D_0 increases in a row of following nitrides: HfN → VN → TiN (calculated values (mol/s): $6.5 \cdot 10^{-6}$ for HfN, $28.7 \cdot 10^{-6}$ for VN, $48.5 \cdot 10^{-6}$ for TiN).

It is known that the experimental determination of diffusion parameters of nitrogen in a solid state is an extremely difficult task, especially providing such an experiment at high pressure. Therefore, application of data on the refined crystal structures of nitrides is quite promising for this purpose, but it only gives a general idea of the nature of diffusion processes in the above-mentioned systems, and to some extent allows these systems to be compared.

3.2. MeC Crystal Structure of PcBN Composites

3.2.1. XRD Study of MeC Phases of Group IV Metals (TiC, ZrC, HfC)

XRD phase analysis of diffraction peaks obtained from HPHT sintered at different temperatures composites of cBN–*Me*C–Al systems where *Me* = Ti, Zr, Hf has revealed that barothermal processing of the charge leads to the formation of additional phases in samples. In particular, existence of two reaction products, namely, isostructural MeB_2 diborides (TiB_2, ZrB_2 or

HfB_2) and a small amount of AlN (Table 7) was detected in the composites obtained at temperatures higher than 2000 °C in addition to initial components of the charge (cBN, *Me*C, Al). Moreover, the splitting of *Me*C reflections is observed on the diffraction patterns of samples sintered at 1900–2150 °C (Fig. 4), which may indicate the formation of a new phase isostructural to the original *Me*C carbide (*Me*C′ arbitrary symbol for these systems). *Me*C′ monocarbides in their pure form present in the final products of HPHT sintering, and at lower temperatures, as noted above, *Me*C and *Me*C′ carbides sometimes coexist (Table 7).

Considering the presence of two carbides in the composites, the lattice parameters a of *Me*C and *Me*C′ were calculated (Table 7). Figure 11 clearly demonstrates a tendency of lattice parameter a to decrease around 2000 °C of sintering temperature, which is the typical feature of $a(T)$ dependences.

In order to find out the reasons that cause a decrease in lattice parameters of *Me*C phases in the products of HPHT sintering of cBN–{TiC, ZrC, HfC}–Al mixtures (Table 7, Fig. 11), a refinement of the crystal structure of each carbides (*Me*C and *Me*C′) was carried out within NaCl-type structure model at the first stage of research. Calculations provided have shown that sintering temperature makes a significant impact on the crystal structure of *Me*C′ carbides, while *Me*C carbides are characterized by the presence of a small fraction of vacancies in their metal sublattice only.

Previously [40], we have assumed that such jump-like change in the lattice parameter in HPHT-sintered cBN–HfC–Al samples is caused by the dissolving of Al in HfC lattice. That is why this assumption was accepted in the present refinement procedure. Therefore, *Me*C′crystal structure refinement was carried out within the framework of the following model $Fm3m$ (No. 225):

$$4(q_1 Me + (1 - q_1)\text{Al}) \text{ are placed in } 4a \text{ (0 0 0)},$$
$$4q_2\text{C} \text{ are placed in } 4b \text{ (0.5 0.5 0.5)},$$
$$-4q_3 Me \text{ are placed in } 4a \text{ (0 0 0)};$$

here, q_1 is the occupation factor of the regular points system of $4a$ with metal atoms, q_3 is part of the vacancies in it (according to calculation, q_1 and q_3 are less than 1), and q_2 is the occupation factor of regular points system of $4b$ with carbon atoms (the calculation shows that $q_2 = 1$). Refinement of occupation factors of q_1, q_2, and q_3 positions, as well as temperature corrections B led to a satisfactory agreement between the experimental and calculated values of reflection intensities (reliability factors R_B did not exceed 0.04). Data obtained on the calculated composition of these carbides are listed in Table 7. Calculations also show that Al atoms almost do not dissolve in *Me*C carbides, but the metal sublattice of *Me*C accumulates a small amount of vacancies. Figure 11 illustrates the change of *Me*C lattice parameters and Al content in carbide phases.

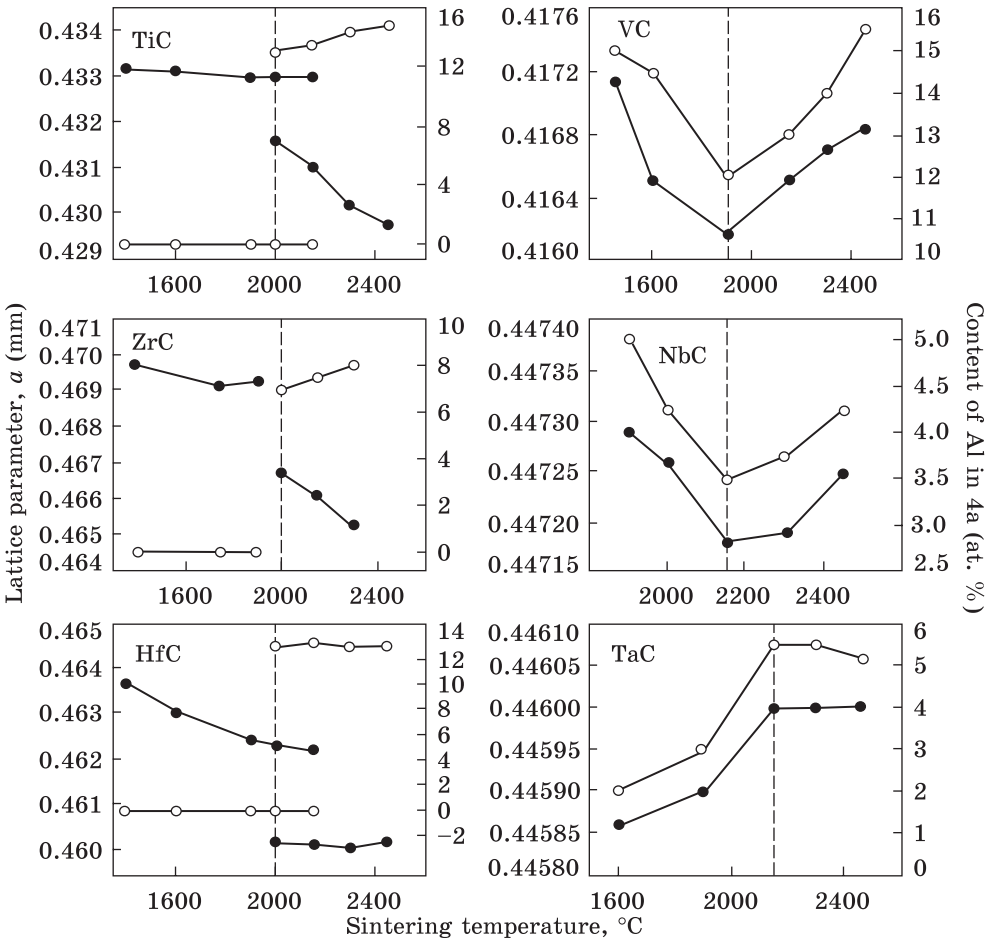

Fig. 11. Temperature dependence of *Me*C lattice parameters of on sintering temperature of cBC–*Me*C–Al charge (black circles) and the fraction of Al atoms in 4*a* position of these carbides (white circles)

In order to improve the convolution between calculated and experimental values of the reflection intensities (to reduce the reliability factor R_B), results of the study of nitrogen-atoms' embedding in the interstices of nitride crystal lattices were additionally taken into account. Therefore, the final refinements of *Me*C and *Me*C′ crystal structures were carried out in the model of a modified NaCl-type structure, taking into account the previous data on Al solubility in *Me*C′ phases. As an example, Table 8 contains the result of crystal structure calculation of titanium carbide, which exists in composites sintered at 1900 and 2450 °C (TiC and TiC′ phases) (Table 7, Fig. 11).

Thus, structural calculations show that aluminium does not dissolve in *Me*C carbides (*Me* = Ti, Zr, Hf), forming in composites sintered at

Table 7. **Phase composition of cBN–*Me*C–Al composites HPHT sintered at 7.7 GPa and**

Sintering temperature T, °C	Phase composition	Lattice parameter a, nm
	Composites of cBN–TiC–Al system	
1600	cBN(64)[1] + TiC(33) + Al(3)	0.43338
1900	cBN(64) + TiC(34) + TiB_2(1) + AlN(1)	0.43298
2000	cBN(63) + TiC(34) + TiB_2(2) + AlN(1)	0.43310
2150	cBN(61) + TiC(24) + TiC'(10) + TiB_2(4) + AlN(1)	0.43298[2,3]/0.43103
2300	cBN(61) + TiC′(26) + TiC(6) + TiB_2(6)+AlN(1)	0.43267/0.43017
2450	cBN(61) + TiC′(31) + TiB_2(7) + AlN(1)	0.42978
	Composites of cBN–ZrC–Al system	
1750	cBN(62) + ZrC(36) + Al(2)	0.46916
1900	cBN(60) + ZrC(40)	0.46923
2000	cBN(62) + ZrC′(32) + ZrB_2(5) + AlN(1)	0.46675
2150	cBN(62) + ZrC′(29) + ZrB_2(8) + AlN(1)	0.46604
2300	cBN(62) + ZrC′(29) + ZrB_2(8) + AlN(1) + ZrO_2 ?	0.46525
	Composites of cBN–HfC–Al system	
1600	cBN(64) + HfC(33) + Al(3)	0.46302
1900	cBN(65) + HfC(34) + HfB_2(1)	0.46241
2000	cBN(62) + HfC(24) + HfC′(6) + HfB_2(8)	0.4623/0.46015
2150	cBN(62) + HfC′(18) + HfC(10) + HfB_2(10)	0.4622/0.46015
2300	cBN(62) + HfC′(26) + HfB_2(12) + AlN ?	0.4601
2450	cBN(62) + HfC′(26) + HfB_2(12) + AlN ?+Cgr	0.46021
	Composites of cBN–VC–Al system	
1600	cBN(65) + VC(34) + Al_2O_3(1)	0.41714
1900	cBN(65) + VC(35)	0.41652
2000	cBN(65) + VC(35) + VB_2 ?	0.41617
2150	cBN(65) + VC(33) + VB_2 ?	0.41651
2300	cBN(65) + VC(34) + Al_2O_3(1)	0.41671
2450	cBN(65) + VC(34) + Al_2O_3(1)	0.41684
	Composites of cBN–NbC–Al system	
1900	cBN(64) + NbC(32) + NbB_2(3) + AlN(1)	0.44729
2000	cBN(65) + NbC(31) + NbB_2(4)	0.44726
2150	cBN(62) + NbC(35) + NbB_2(3) + AlN(1)	0.44718
2300	cBN(62) + NbC(33) + NbB_2(5)	0.44719
2450	cBN(62) + NbC(33) + NbB_2(5)	0.44725
	Composites of cBN–TaC–Al system	
1600	cBN(64) + TaC(36)	0.44586
1900	cBN(65) + TaC(35)	0.4459
2150	cBN(62) + TaC(35) + TaB_2(4)	0.4460
2300	cBN(62) + TaC(33) + TaB_2(5)	0.4460
2450	cBN(62) + TaC(33) + TaB_2(5)	0.4460

[1] In parentheses, the content of phases is given in vol.%; [2] Lattice parameters of differ *Me*C; [4] Lattice deformation of nitrides in composites is estimated in relation to corre spond (contains 4 atoms)

crystal structure characteristics of their *Me*N phases

Number of atoms in position				Carbide content, at.%			
Me in 4*a*	Al in 4*a*	C in 4*b*	N in 24*e*	Ti	Al	C	N
Composites of cBN–TiC–Al system							
4.00	0.00	4	0.52	47.0	0	47.0	6.1
4.00	0.00	4	0.44	47.4	0	47.4	5.2
3.86	0.00	4	0.37	46.9	0	48.6	4.5
3.77	0.00	4	0.79	44.0	0	46.8	9.1
3.41	0.59	4	0.47	38.8	7.3	48.4	5.7
3.41	0.59	4	0.32	39.3	7.3	49.3	4.0
Composites of cBN–ZrC–Al system							
4.00	0	4	0.41	47.6	0	47.6	4.9
4.00	0	4	0.80	45.4	0	45.4	9.1
3.80	0	4	0.01	48.7	0	51.2	0.0
3.70	0.30	4	0.19	45.2	3.7	48.8	2.3
3.70	0.30	4	0.19	45.2	3.7	48.8	2.3
Composites of cBN–HfC–Al system							
4.00	0	4	2.32	38.7	0	38.7	22.5
3.87	0	4	2.12	38.7	0	40.0	21.2
3.85	0	4	0.00	49.0	0	51.0	0.0
3.47	0.53	4	0.77	38.7	6.1	46.2	8.9
3.48	0.52	4	0.61	39.7	6.1	47	7.1
3.48	0.52	4	1.07	37.6	5.8	44.6	12
Composites of cBN–VC–Al system							
3.4	0.6	4	4.00	24.4	4.5	29.0	42.0
3.42	0.58	4	4.22	24.7	4.3	29.1	41.7
3.52	0.48	4	3.47	26.3	4.4	30.7	38.6
3.48	0.52	4	3.22	26.7	4.4	31.2	37.7
3.44	0.56	4	3.71	27.8	4.5	32.3	35.3
3.38	0.62	4	3.57	28.1	4.6	32.7	34.6
Composites of cBN–NbC–Al system							
3.80	0.20	3.20	1.42	44.0	2.4	37.1	16.5
3.83	0.17	3.3	1.42	43.9	1.9	37.9	16.3
3.86	0.14	3.28	0.93	44.3	2.2	41.1	12.4
3.85	0.15	3.28	0.88	47.2	1.9	40.2	10.7
3.83	0.17	3.19	1.50	44.1	1.9	36.7	17.2
Composites of cBN–TaC–Al system							
3.92	0.08	3.80	0.21	48.9	1	47.4	2.6
3.88	0.12	3.89	0.01	49.2	1.5	49.2	0
3.78	0.22	4	0.02	47.0	2.7	49.7	0
3.81	0.19	4	0	47.7	2.3	50.0	0
3.84	0.16	4	0	48.0	2.0	50.0	0

ent carbide compositions are listed; [3] Data on the crystal structure are given for carbide ing valuesin the charge; [5] 4a position is completely occupied by corresponding Me atoms

1600–2000 °C, but metal lattice of these carbides accumulates a small amount of vacancies (Table 7). At the same time, Al is not dissolved in *Me*C′ at higher sintering temperatures (2000–2450 °C). In addition, it was shown that *Me*C and *Me*C′ carbides could dissolve nitrogen, which is formed during partial decomposition of cBN nitride. Data on the complete composition of *Me*C and *Me*C′ phases obtained by structural calculations are listed in Table 7.

3.2.2. XRD Study of Group V Carbides MeC (Me = V, Nb, Ta)

Results of qualitative and quantitative XRD phase analysis of diffraction patterns obtained from composites of cBN–*Me*C–Al (*Me* = V, Nb, Ta) systems sintered in certain temperature ranges showed that barothermal processing of initial charge leads to the formation of a small amount of NbB_2 or TaB_2, and vanishingly small amounts of AlN, VB_2 and/or Al_2O_3 (Table 7).

However, even though the phase composition is almost the same (cBN–NbC–Al system) or slightly changes with sintering temperature (cBN–VC–Al and cBN–TaC–Al systems), lattice parameters of these *Me*C carbides are

Table 8. **TiC crystal structure calculations (cBN–TiC–Al charge)**

TiC of sintered at в 1900 °C composite (modified NaCl type structure)					
Atom	Position	Occupation	*X*	*Y*	Z
Ti	4*a*	1.000(1)	0	0	0
C	4*b*	1.000(1)	0.5	0.5	0.5
N	24*e*	0.073(3)	0.320	0	0
Space group			*Fm3m* (No. 225)		
Lattice parameter *a*, nm			0.43298(7)		
Temperature coefficient *B*, nm^2			$1.03(3)\cdot10^{-2}$		
Phase composition calculated, at.%			47.4Ti + 47.4C + 5.2N		
Reliability factor, R_B			0.011		
TiC′ of sintered at в 2450 °C composite (modified NaCl type structure)					
Atom	Position	Occupation	*X*	*Y*	Z
Ti	4*a*	0.852(1)	0	0	0
Al	4*a*	0.148(1)	0	0	0
Ti_vac	4*a*	–0.055(4)	0	0	0
C	4*b*	1.000(1)	0.5	0.5	0.5
N	24*e*	0.140(3)	0.320	0	0
Space group			*Fm3m* (No. 225)		
Lattice parameter *a*, nm			0.42978(9)		
Temperature coefficient *B*, nm^2			$1.34(1)\cdot10^{-2}$		
Phase composition calculated, at.%			39.4Ti + 7.3Al + 49.3C + 4.0N		

changed significantly (Fig. 11). Moreover, this change is almost monotonous, *i.e.*, there is no clear two-phase existence region of two different *Me*C and *Me*C′ phases in contrast to carbides of group IV metals (Table 7, Fig. 11). Meanwhile, the mentioned variation in the lattice parameter of *Me*C carbides of group V, taking place with a change in sintering temperature (Fig. 11), indicates certain transformations of their crystal structure.

To refine the crystal structure of *Me*C carbides of this group, a model of the modified NaCl-type structure was also applied. This model was described in detail above for *Me*C′ phases of group IV and is presented in Table 8 as calculation results for TiC′. In this model, refinement of the occupation factor of corresponding positions (q_1, q_2, and q_3) by metal atoms, aluminium, carbon, and nitrogen atoms in relation to the refinement of isotropic temperature factor B led to a good agreement between the experimental and calculated values of the reflection intensities (reliability factors R_B did not exceed 0.01). Table 7 contains the number of atoms in the correct points systems and the full composition of *Me*C phases of group V metals (*Me* = VC, NbC, TaC) calculated from these data, while the temperature dependence of the calculated Al content in these carbides is presented in Fig. 11.

Calculations provided have also shown that in TaC carbide the nitrogen atoms only occupy vacancies of the carbon sublattice (4*b* position). However, in VC and NbC carbides, nitrogen atoms occupy the position of 24*e*, where a significant part of carbon atoms migrates from position 4*b* in NbC (Table 7).

3.2.3. Character of MeC (Me = Ti, Zr, Hf, V, Nb, Ta) Interaction with Al and N

In the detailed XRD study described above it was established that the crystal structure of *Me*C monocarbides of metals of IV and V groups is well described by a modified NaCl-type structure with nitrogen atoms embedded in the interstices of carbide lattice. At certain modes of HPHT sintering, partial replacement of *d*-transition metal atoms by Al atoms also occurs. General nature of the placement of *d*-metal, aluminium, carbon, and nitrogen atoms is presented in Fig. 12.

Certain differences between carbides of groups IV and V relate only to the occupation degree of corresponding positions of their crystal structures with aluminium and nitrogen atoms, depending on the temperature of HPHT sintering of the cBN–*Me*C–Al composite (Fig. 11, Table 7). That is, the accumulation of Al atoms of the binder formed between the charge and nitrogen atoms released as a result of partial decomposition of cBN is the main feature of *Me*C carbides exposed to barothermal processing.

Results obtained on the dissolution of Al in *Me*C crystal lattice at high pressure (Table 7) were compared with the available data on isothermal cross-sections of cBN–*Me*C–Al ternary systems, plotted from the results

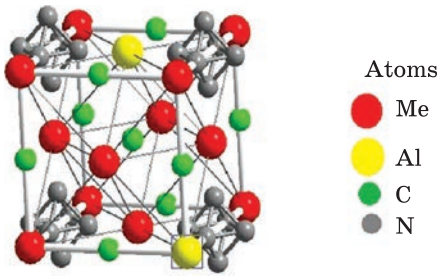

Fig. 12. Arrangement of *Me*, Al, C, and N atoms in the *Me*C-based structure of solid solutions

of studies of alloys produced by the arc melting method at normal pressure. It turned out that under normal conditions, the solubility of aluminium in TiC, ZrC, HfC, VC, NbC, TaC crystal lattices is not observed, at least in the studied temperature range, which is determined by the melting temperature of Al.

However, the interaction mechanism of Al with one of *Me*C monocarbides (TiC) at normal pressure is covered in detail in Ref. [53], where the role of the interphase transition layer between these phases is considered. It is shown that TiC, instead of a direct reaction with aluminium melt at the nucleation temperature of the main crystallization centres (720 °C), actually releases Ti atoms into this melt, contributing to the formation of an interphase transition layer containing Ti and Al. At the same time, the ratio of C to Ti in TiC is increased after the release of Ti atoms due to the formation of vacancies in the metal sublattice, decreasing Ti content in carbides [53]. Obviously, Al atoms from the melt will penetrate into the defective TiC lattice due to diffusion, forming a solid interstitial solution.

Thus, the formation of vacancies plays a decisive role in the interaction of Al with *Me*C phases. Previously [54], we have shown that the number of vacancies in *Me*C lattices of carbides sintered at 700 °C forms mechanically alloyed powders of metal and carbon nanotubes increases monotonically in the series HfC → ZrC → TiC → TaC → NbC → VC (Fig. 13). Similar dependence is observed for the number of vacancies in the metal sublattice of group IV carbides (TiC, ZrC, and HfC) accumulated in crystal structures of these carbides at HPHT sintering at temperature lower than the formation point of aluminium solid solutions (≈2000 °C). It should be mentioned that such speculations do not make sense for composites of group V carbides since the aluminium solid solutions in VC, NbC, and TaC already exist at all sintering temperatures studied (Table 7, Fig. 11).

Undoubtedly, the diffusion mechanism described for TiC in Ref. [53] also takes place when Al interacts with other *Me*C monocarbides. That is the formation of Al solid solutions in carbide is preceded by the formation of vacancies in it. It can also be assumed that free Al atoms, diffusing through the sample at HPHT sintering, eventually occupy all the vacancies of metal sublattice in the carbide formed. This means that the number of Al atoms that can be placed in the carbide structure is directly related to the number of vacancies formed in it, which is primarily determined by the energy of breaking *Me*–C bonds.

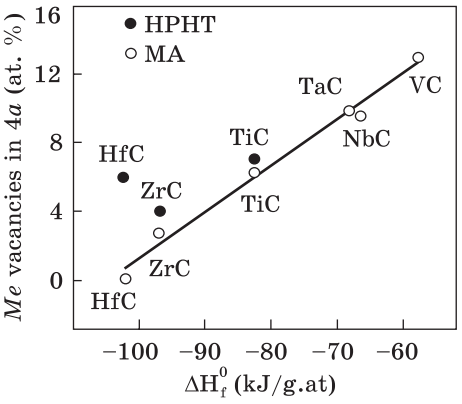

Fig. 13. The number of vacancies accumulating in the metal sublattices of *Me*C phases after mechanical alloying of metal powders and carbon nanotubes (6 h of processing in a ball mill and compaction at 700 °C; open circles) and at HPHT sintering of cBN–*Me*C–Al composites at a temperature of ≈2000 °C (full circles)

Values of the dissociation energy of *Me*–C thermochemical bonding for all IV–V group monocarbides were determined in Ref. [55] by the resonance two-photon ionization method. Data obtained in Ref. [55] were used to analyse the degree of replacement of metal atoms by Al atoms in 4*a* position of the carbide structure. Taking into account that the solubility of Al in carbides is drastically increased at high sintering temperatures (Table 7, Fig. 11), the dependence mentioned was plotted for samples sintered at 2300 °C (Fig. 14).

Figure 14 clearly demonstrates that the content of Al dissolved in *Me*C does correlate with the energy of thermochemical destruction of their *Me*–C bonds. Probability of formation of vacancies in the metal sublattice, which can be and are finally occupied by Al atoms from the reaction zone, is higher if *Me*–C bond is weaker. The dependence of Al content in HPHT sintered *Me*C carbides (and, therefore, the preliminary formation of vacancies in them) on the energy of destruction of *Me*–C bonds explains the experimentally observed decre-ase in the number of vacancies in the series TiC → HfC → ZrC (Table 7, Fig. 13), and not in the series TiC → ZrC → HfC, as is observed for mechanically alloyed *Me*C carbides (Fig. 13).

On the other hand, the destruction of *Me*–C bonds also leads to the release of a certain amount of carbon atoms, resulting in the formation of vacancies in its sublattice. Carbon atoms can migrate along the carbide lattice together with nitrogen atoms. This process is proved by the data obtained on the vacancies in 4*b* position (Table 7). Migration of N atoms released during cBN decomposition leads to its continuous migration along the vacancies of both metal and carbon sublattices of the *Me*C crystal structure until they finally embed into the monocarbide lattice. That is,

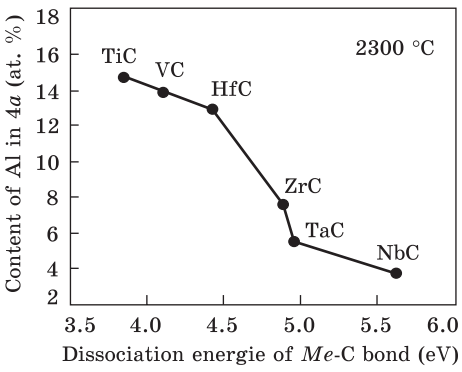

Fig. 14. Dependence of Al content in the metal sublattice of *Me*C structure (4*a* position, full circles) existing in cBN–*Me*C–Al samples sintered at 2300 °C on the energy of thermochemical dissociation of *Me*–C bonds

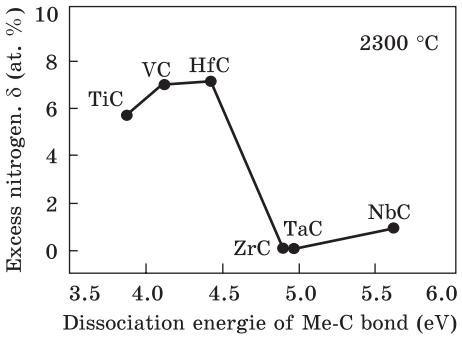

Fig. 15. The excess N in *Me*C structure of cBN–*Me*C–Al sintered at 2300 °C *vs.* the energy of thermochemical dissociation of *Me*–C bonds

the amount of nitrogen accumulated by the carbide crystal lattice may also depend on the energy of thermochemical destruction of *Me*–C bond. This assumption was confirmed by data on nitrogen solubility in *Me*C lattices at sintering temperature of 2300 °C (Fig. 15).

The number of vacancies accumulated by carbides of group IV at HPHT sintering of cBN–*Me*C–Al composites at a temperature of ≈2000 °C correlates with the content of Al dissolved in them at high temperatures (≈2450 °C, Table 9). Taking into account the data obtained on Al content in *Me*C′ carbides (Table 7), the limit compositions of these solid solutions can be conventionally represented as Ti_6AlC_7, Zr_7AlC_8 and Hf_8AlC_9. Considering this, the solid-phase reactions taking place at HPHT sintering above 2000 °C can be written as

$$2cBN + nMeC + 3Al = Me_{n-1}AlC_n + MeB_2 + 2AlN,$$

where n = 6, 7 and 8 for Ti, Hf and Zr, respectively.

In our opinion, the temperature detected at the beginning of this solid-phase reaction (around 2000 °C) is caused by the presence of liquid Al in the reaction zone.

Table 9. **Composition of compounds with TiC, ZrC and HfC**

Initial charge	Processing mode	Lattice parameter *a*, nm	Composition of *Me*C′/*Me*C[3] calculated, at.%	Compound
*Me*C′ of HPHT sintered composite				
cBN–TiC–Al[1]	2450 °C	0.42978(9)	41.0Ti + 7.6Al + 51.4C	$Ti_{0.80}Al_{0.15}C$
cBN–ZrC–Al[1]	2300 °C	0.46525(3)	44.4Zr + 5.1Al + 50.5C	$Zr_{0.88}Al_{0.10}C$
cBN–HfC–Al[1]	2450 °C	0.46021(2)	42.8Zr + 6.6Al + 51.2C	$Zr_{0.84}Al_{0.13}C$
*Me*C of sintered composite of mechanically alloyed charge [54]				
Ti–C[2]	6 h. 700 °C	0.4301(1)	48.3Ti + 51.7C	$Ti_{0.97}C$
Zr–C[2]	5 h. 700 °C	0.4655(1)	49.6Zr + 50.4C	$Zr_{0.99}C$
Hf–C[2]	6 h. 700 °C	0.4588(1)	50.0Hf + 50.0C	HfC
*Me*C obtained traditionally				
TiC	—	0.4327	51.3Ti + 48.7C	$TiC_{0.95}$
ZrC	—	0.4693	51.3Zr + 48.7C	$ZrC_{0.95}$
HfC	—	0.4619	50.0Hf + 50.0C	$HfC_{0.95}$

[1] Charge content (vol.%) 60cBN + 35*Me*C + 5Al; [2] Charge content (at.%) 50*Me* + 50C; [3] *Me*C composition is given without taking into account the content of nitrogen

Thus, *Me*C carbides of the charge at HPHT sintering of cBN–*Me*C–Al composites form $Me_{1-x}Al_xCN_\delta$ solid solutions under certain processing conditions. The composition of these solid solutions was determined by XRD studies.

3.3. Crystal Structure of TiCN Carbonitride in PcBN Composite of cBC–MeCN–Al System

3.3.1. XRD Study of TiCN Phase

According to the XRD study, the composition of initial titanium carbonitride is $TiC_{0.5}N_{0.5}$ due to the position of lattice parameter on the Vegard's plot for TiC and TiN. For convenience, let us denote this carbonitride as TiCN in the following sections.

Diffraction patterns obtained from HPHT sintered composites of the cBN–TiCN–Al system at several temperatures indicate that the barothermal processing of initial charge leads to the formation of additional phases, *i.e.*, products of the reaction of charge components, namely, TiB_2 and a small amount of AlN (Table 10). Moreover, all diffraction peaks of TiCN in the diffraction pattern of a sample sintered at 2150 °C are split as in the case of cBN–TiC–Al system composites, which may indicate the formation of two isostructural phases in this specific composite (these phases are conventionally marked as TiCN′ and TiCN, Table 10). Temperature dependences of the refined values of the TiCN′ and TiCN lattice parameters are shown in Fig. 16, which demonstrate a significant jump of the crystal lattice parameter in the vicinity of sintering temperature of 2150 °C.

To refine the crystal structure of TiCN carbonitride existing in the products of HPHT sintering, a model of the modified NaCl-type structure described in detail above for *Me*C carbides was also applied. However, it should be noted that, since the meanings of XRD scattering power for carbon and nitrogen is quite close, it is possible to talk only about their total contribution to corresponding positions. Total carbonitride compo-

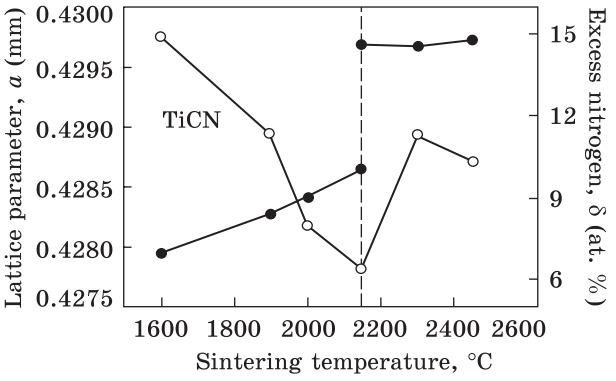

Fig. 16. Temperature dependencies of TiCN lattice parameter on the sintering temperature of cBC–TiCN–Al charge (full circles) and the fraction of Al atoms in 4*a* position of this carbonitride (open circles)

Table 10. **The phase composition of cBN–TiCN–Al composites HPHT sintered at 7.7 GPa and crystal structure characteristics of their TiCN phase**

Sintering temperature T, °C	Phase composition	Lattice parameter a, nm	Number of atoms in position				Content of carbonitride, at.%			
			Ti in 4*a*	Al in 4*a*	C + N in 4*b*	N + C in 24*e*	Ti	Al	C	N
1600	cBN(64)[1] + TiCN′(33) + + Al(3)	0.42797	3.44	0.56	3.75	2.19	34.7	5.6	20.2	39.5
1900	cBN(63) + TiCN′(34) + + TiB_2(2) +AlN(1)	0.42845	3.44	0.56	3.79	1.61	36.6	6.0	21.3	36.1
2000	cBN(63) + TiCN′(34) + + TiB_2(2) +AlN(1)	0.42829	3.44	0.56	3.74	1.19	38.4	7.0	22.4	32.8
2150	cBN(63) + TiCN′(25) + + TiCN(9) + TiB_2(2) + + AlN(1)	0.42865/0.43043[2]	3.43	0.57	3.79	1.09	38.9	6.4	22.7	32.0
2300	cBN(63) + TiCN(34) + + TiB_2(2) + AlN(1)	0.42967	3.82	0.18	3.96	1.34	39.8	1.9	21.9	36.3
2450	cBN(61) + TiCN(31) + + TiB_2(7) + AlN(1)	0.42972	3.82	0.18	3.87	1.31	40.4	2.0	22.2	35.3

[1] In parentheses, the content of phases is given in vol.%; [2] Lattice parameters of carbonitride phases of different content are presented

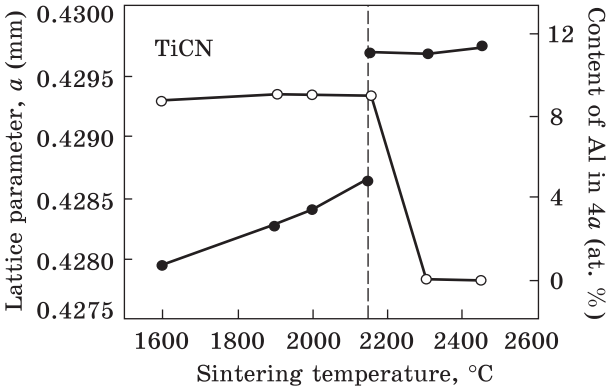

Fig. 17. Temperature dependencies of TiCN lattice parameter on sintering temperature of cBC–TiCN–Al charge (full circles) and excess nitrogen content (open circles)

Table 11. **Crystal structure calculations for TiCN of cBN–TiCN–Al HPHT sintered composite**

TiCN′ phase of composite sintered at 1900 °C (modified NaCl type structure)					
Atom	Position	Occupation	*X*	*Y*	Z
Ti	4*a*	0.859(1)	0	0	0
Al	4*a*	0.141(1)	0	0	0
C + N	4*b*	0.938(1)	0.5	0.5	0.5
N + C	24*e*	0.050(4)	0.280	0	0
Space group			*Fm*3*m* (No. 225)		
Lattice parameter *a*, nm			0.42845(7)		
Temperature coefficient *B*, nm^2			$2.05(3)\cdot10^{-2}$		
Phase composition calculated, at.%			38.5 Ti+6.3Al+22.4C+32.8N		
Reliability factor R_B			0.005		
TiCN phase of composite sintered at 2300 °C (modified NaCl type structure)					
Atom	Position	Occupation	*X*	*Y*	Z
Ti	4*a*	0.901(1)	0	0	0
C + N	4*b*	0.969(4)	0.5	0.5	0.5
N + C	24*e*	0.050(3)	0.280	0	0
Space group			*Fm*3*m* (No. 225)		
Lattice parameter *a*, nm			0.42978(9)		
Temperature coefficient *B*, nm^2			$1.72(1)\cdot10^{-2}$		
Phase composition calculated, at.%			41.1Ti + 22.8C + 36.1N		
Reliability factor, R_B			0.013		

sition was determined considering the carbon content in TiCN crystal lattice does not change at sintering. Crystal structure refinement results of TiCN carbonitride existing in two HPHT sintering products are listed in Table 11.

Using the data obtained during structural calculations, the total composition of TiCN in sintering products of the cBN–TiCN–Al charge was determined (Table 10). The numbers of Al dissolved in carbonitrides and excess nitrogen occupying 24*e* positions are presented in Figs. 16, 17.

4. Discussion: Compilation of the Data Obtained on Crystal Structure Features of *Me*N and *Me*C/TiCN Phases Formed at HPHT Sintering of cBN–*Me*N–Al, cBN–*Me*C–Al and cBN–TiCN–Al Composites

4.1. Interaction of d-Transition Metals of IV–V Groups Carbides and Nitrides with Nitrogen

XRD studies have revealed that HPHT sintered composites of cBN–*Me*N–Al, cBN–*Me*C–Al, and cBN–TiCN–Al systems are characterized by transformation of the crystal structures of *Me*N mononitrides and *Me*C/TiCN monocarbides of *d*-transition metals. This transformation is described as an additional 24*e* position in crystal structure, which is occupied by nitrogen atoms in a certain manner. At the same time, additional nitrogen atoms N(2) are placed on vertices of the octahedron, centre of which is occupied or rather not occupied by atoms from the main 4*b* position, *i.e.*, N(1) atoms in *Me*N nitrides or C atoms in *Me*C carbides. In general, atoms of the components in modified NaCl-type structure are placed according to positions of $Fm3m$ (No. 225) space group as follows:

$$4(q_1 Me + (1 - q_1)\text{Al}) \text{ are placed in } 4a \text{ (0, 0, 0)},$$

$$4q_2\text{C/N(1) are placed in } 4b \text{ (0.5, 0.5, 0.5)},$$

$$-4q_3 Me \text{ are placed in } 4a \text{ (0, 0, 0)},$$

$$24q_4\text{N(2) are placed in } 24e \approx (0.320, 0, 0);$$

here, q_1 is the occupation factor of 4*a* regular-points' system by metal atoms; q_3 is the vacancies' fraction in 4*a* regular-points' system; q_2 is the occupation factor of 4*b* regular-points' system by C atoms in carbides or N atoms in nitrides; q_4 is the occupation factor of 24*e* regular-points' system N atoms.

Providing structural calculations based on all available diffraction peaks of the *Me*N or *Me*C phases, q_1, q_2, q_3, and q_4 parameters were refined followed by the refinement of the composition of compound (Tables 4, 7, and 10) and the isotropic temperature factor B. Reliability factor R_B did not exceed 0.02 for this set of calculation and certifies its correctness. The arrangement of the component atoms in this modified NaCl-type crystal structure is presented in Fig. 18.

The existence of additional nitrogen atoms in the structures of *Me*N nitrides and *Me*C carbides established by XRD structural analysis is well described within the framework of the atomistic diffusion model proposed by D.G. Sangiovanni *et al.* [51]. This process controls the spontaneous formation of the Frenkel pairs from interstitial nitrogen atoms N(2) and va-

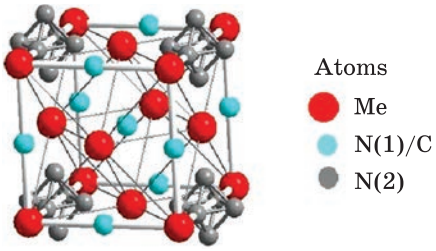

Fig. 18. Arrangement of component atoms within the model of the modified NaCl-type structure (space group *Fm*3*m*)

cancies of the crystal lattice N(1) in nitrides (or vacancies of C atoms in carbides). That is, the decomposition of cBN and *Me*N/TiCN at barometric processing of composites leads to the formation of diffusion flows of nitrogen atoms. Due to the temperature gradient in the reaction zone of HPHT sintering, the nitrogen flows usually move towards the sample surface, where a fraction of atoms leaves the sintered composite as N_2 gas, but a certain part of N atoms is embedded into the crystal lattice of nitride or carbide. This ultimately leads to supersaturation of the samples' surface with nitrogen, which is detected at the refinement of the crystal structures of the *Me*N and *Me*C phases.

It was logical to assume that the fraction of nitrogen atoms embedded into *Me*N and *Me*C lattices at HPHT sintering depends on the nature of interaction and strength of the bond between atoms of nitrogen and d-metals. The analysis provided has shown that the amount of excess nitrogen

Table 12. **Excess nitrogen in cBN–*Me*N–Al and cBN–*Me*C–Al composites**

Nitride	Formation enthalpy, kJ/mol	Excess nitrogen, at.%		Dissociation energy, kJ/mol
		Sintering temperature, °C		
		2150	2300	
HfN	–374	7.06	9.17	1461
ZrN	–365	7.706	8.47	1437
TiN	–323	5.976	5.60	1261
VN	–298	4.15	3.92	1197
TaN	–252	—	—	1505
NbN	–213	3.51	2.86	1420

Carbide	*Me*–C bond breaking energy, eV	Al content in 4*a* position, at.%		Excess nitrogen, at.%	
		Sintering temperature, °C			
		2150	2300	2150	2300
NbC	5.62	3.5	3.75	0	0.9
TaC	4.975	5.5	5.5	0	0
ZrC	4.892	7.5	7.5	2.3	0
HfC	4.426	13	13	8.9	7.1
VC	4.109	14	14	7	7
TiC	3.857	14.8	14.75	9.1	5.7
TiCN	3.857 ?	14.0	14.5	7.0	9

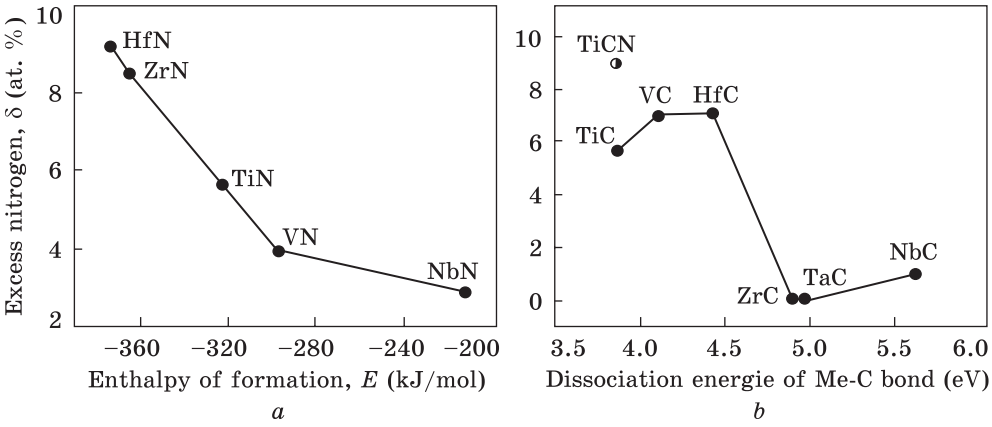

Fig. 19. Dependences of excess nitrogen in the structures of *Me*N phases on the enthalpy of their formation (*a*) and excess nitrogen in the structures of *Me*C phases on the energy of thermochemical dissociation of *Me*–C bonds (*b*) (sintering temperatures are 2000–2150 °C)

accumulated by *Me*N structures determined by structural calculations correlates with the enthalpy of formation of these nitrides, while the amount of excess nitrogen accumulated by *Me*C structures correlates with the dissociation energy of *Me*–C thermochemical bond. Experimentally obtained data on the amount of excess nitrogen in *Me*N and *Me*C phases at high sintering temperatures are listed in Table 12 and presented in Fig. 19.

Such difference in definition of the criteria for assessing the content of excess nitrogen for *Me*N and *Me*C is not surprising since it is determined by different mechanisms of interaction with nitrogen. According to data present in literature [52], dissociation of *Me*N at normal pressure takes place by evaporation, forming a large number of vacancies in the nitrogen sublattice, while the metal sublattice remains almost undefective. That is, the formation of nitrogen-saturated nitrides is probably caused by the binding energy of new *Me*–N bonds, which to some extent is due to the formation enthalpy of corresponding nitride. The well-known

Table 13. **Activation energy of nitrogen atoms diffusion in HPHT sintered composites of cBN–TiN–Al, cBN–TiC–Al and cBN–TiCN–Al systems calculated using the Arrhenius equation**

Composite	Temperature range at calculations, °C	Activation energy of diffusion		Al content in *Me*C, at.%	Excess nitrogen, at.%
		E, kJ/mol	*E*, eV		
cBN–TiN–Al	1850–2300	72.9	3.021	—	12.4–5.6
cBN–TiC–Al	1600–2000	59.4	2.46	—	6.1–4.5
cBN–TiC–Al	2150–2450	35.6	1.39	≈7.3	5.7–4.0
cBN–TiCN–Al	1600–2000	48.2	2.00	≈6.2	14.5–7.8

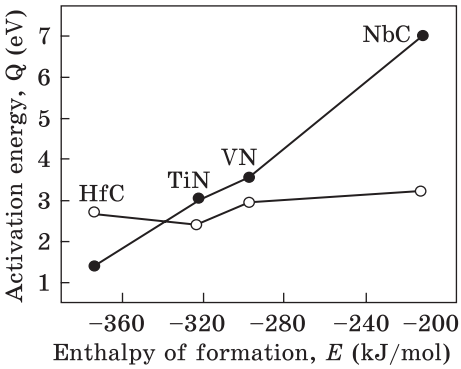

Fig. 20. Activation energy of nitrogen diffusion for *Me*N phases *vs*. the enthalpy of their formation: full circles — our experimental data for HPHT sintered materials; open circles — literature data [56]

mechanism of *Me*C decomposition at normal pressure consists in breaking the *Me*–C bonds with formation of vacancies both in metal and in carbon sublattices of carbides. Naturally, in this case, the fraction of nitrogen accumulated in the carbide lattice can be correlated with the available number of vacancies in it, *i.e.*, with the energy of thermochemical dissociation of *Me*–C bonds.

Considering that the aligned diffusional movement of nitrogen atoms plays a major role in the formation of crystal structures of the *Me*N and *Me*C phases studied, an attempt was made for the first time to apply the values of excess nitrogen δ determined by XRD structural analysis to define the main parameters of this diffusion process.

The main diffusion parameters, *i.e.*, the activation energy and the mobility of nitrogen atoms were calculated by processing temperature dependences of excess nitrogen determined for existing *Me*N/*Me*C phases in a certain composite (Tables 4, 7, and 10) by the Arrhenius equation. The data obtained in this case are listed in Tables 6 and 13 for titanium-containing compounds.

Calculated parameters of nitrogen diffusion at HPHT sintering (Tables 6 and 13) were compared with the data available in the literature on calculated nitrogen diffusion parameters in transition metal nitrides at normal conditions [56]. A comparison of the diffusion parameters determined for *Me*N was carried out in dependence on the formation enthalpy of corresponding *Me*N (Fig. 20). Figure 20 demonstrates a good agreement between data obtained in this work and Ref. [56].

Considering and comparing the results obtained above on the diffusion parameters of nitrogen atoms in the composites studied (Tables 6 and 12), certain remarks should be made.

Quantitative estimation of diffusion parameters of nitrogen was made for HPHT sintered composites with a volume fraction of cBN higher than 60 vol.%. That is, cBN is not only a source of free nitrogen in the reaction zone but is also an obstacle to the movement of its diffusion flows. Thus, the calculation of nitrogen diffusion parameters in a composite of pure TiN sintered at 7.7 GP gives a significantly lower value of the activation energy of nitrogen diffusion (11.1 kJ/mol) and a higher in-order of magnitude value of the atoms' mobility.

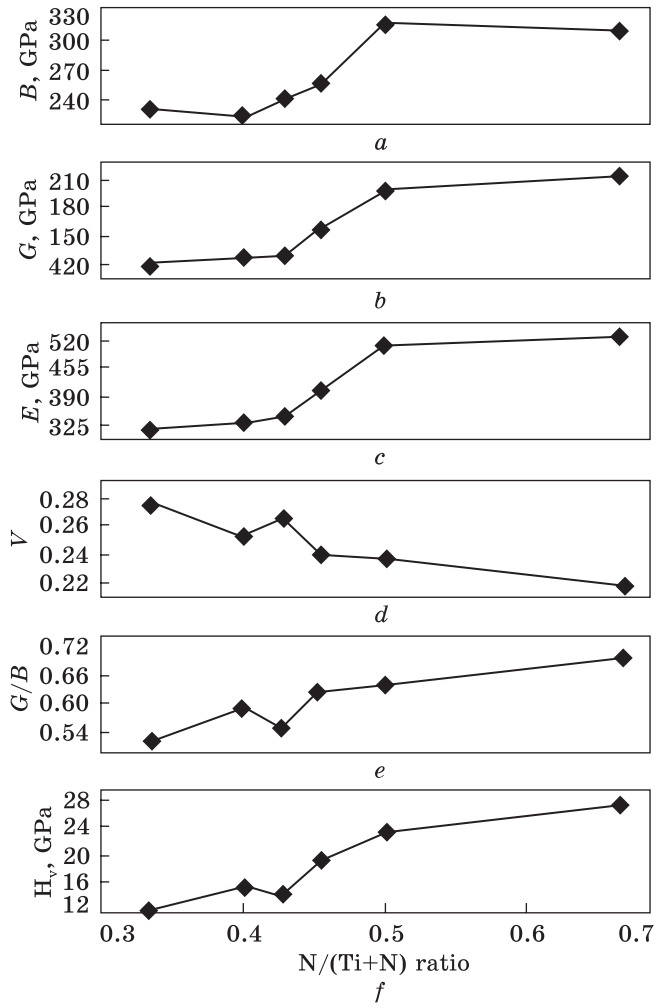

Fig. 21. The bulk modulus, shear modulus, Young's modulus, Poisson's ratio, and hardness *vs.* the excess nitrogen [52]

It was considered that nitrogen diffusion becomes stationary at HPHT sintering. That is, the entire amount of free nitrogen reaches the sample surface and then either leaves it in the form of N_2 gas or is captured by the crystal lattice.

Thus, parameters of nitrogen atom diffusion calculated from the results of refinement of the crystal structures of nitrides or carbides (Tables 6, 12), can be considered as conditional characteristics suitable for comparison the diffusion processes that occur at HPHT sintering of composites with the same volume fraction of charge components and lead to oversaturation with nitrogen of the sample's surface.

S. Yu *et al.* [52] have predicted a relationship between the mechanical properties of the samples and the content of nitrogen in their structure, conducting the first-principles calculations of the electronic structure of

hypothetical and existing compounds of the Ti–N system. Authors of Ref. [52] also have shown that in addition to well-known nitride TiN, stable Ti_3N_2, Ti_4N_3, and Ti_6N_5 phases can exist in this system at atmospheric pressure, and the formation of Ti_2N and TiN_2 is possible too at higher pressure. It was also shown [52] that the nitrogen-rich TiN_2 structure contains encapsulated N_2 dumbbells with an N–N distance of 0.1348 nm at high pressure (60 GPa).

The assumption of S. Yu *et al.* [52] regarding the possible existence of nitrogen-rich TiN_3 phase at high pressure is completely confirmed by our XRD study of the crystal structure of TiN, existing in sintered at 7.7 GPa composites of cBN–TiN–Al system. The real composition of TiN oversaturated with nitrogen almost reaches TiN_2 (Table 4). It is also true that in the TiN structure proposed by us, it is possible to place additional nitrogen atoms in the form of encapsulated dumbbells. Providing an analogy with the data of Ref. [52], these will be nitrogen atoms from position 24*e*, which are located on opposite vertices of the octahedron (Fig. 18). In TiN structures described by us, these distances are about 0.153 nm and not 0.1348 nm, as predicted by S. Yu *et al.* [52] for a pressure of 60 GPa.

S. Yu *et al.* [52] believed that the state of TiN_2 would be stable even at normal pressure and calculated its mechanical properties. For all stable states of the Ti–N system, the values of bulk modulus, shear modulus, Young's modulus, Poisson's ratio, and hardness were estimated. Meanings calculated are presented in Fig. 20 as the dependences on excess nitrogen N/(Ti+N). Authors of Ref. [52] also believe that these calculated values are in good agreement with the experimental data available.

Authors of Ref. [52] also assume that the increase of the number of covalent bonds in the nitrogen-saturated TiN makes a positive impact on some of the main mechanical characteristics (Fig. 21). Therefore, similar changes in the electronic structure undoubtedly occur in other nitrogen-saturated nitrides. That is, we can expect an improvement of mechanical characteristics of most nitrogen-saturated nitrides of *d*-metals of IV–V groups if these phases are placed homogeneously through the volume of the sample even in the presence of second phases (for example, cBN phases). However, in our opinion, nitrogen-saturated nitrides are localized only on the sample surface in HPHT-sintered composites of cBN–*Me*N–Al systems, which means that we can expect just advanced surface characteristics, such as wear resistance, nanohardness, or corrosion resistance.

4.2. Nature of Interaction of MeC Monocarbides of d-Transition Metals f IV–V Groups with Al

The present study has revealed that the amount of Al dissolved in the *Me*N crystal lattice at HPHT sintering of composites of the cBN–*Me*N–Al system cannot be detected by conventional XRD methods. However, par-

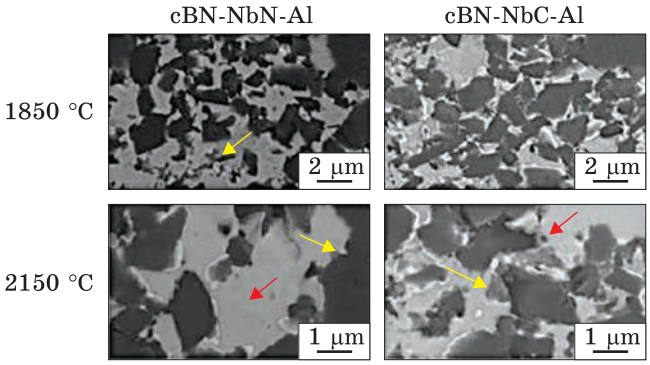

Fig. 22. SEM images of cBN–NbN–Al and cBN–NbC–Al composites obtained at different sintering temperatures [33]

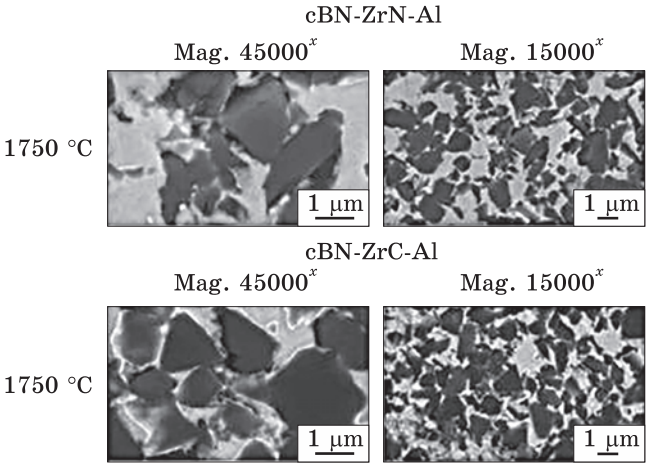

Fig. 23. SEM images of cBN–ZrN–Al and cBN–ZrC–Al composites obtained at sintering temperature of 1750 °C [39, 41]

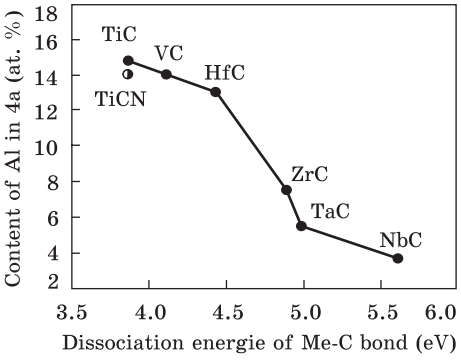

Fig. 24. Dependence of Al content in 4*a* position of *Me*C structure, existing in sintered at 2300 °C samples of cBN–*Me*C–Al composites on the energy of thermochemical dissociation of *Me*–C bonds

tial replacement of *d*-transition metal atoms by Al atoms takes place at certain modes of HPHT sintering in cBN–*Me*C–Al systems. The behaviour and formation conditions of these solid solutions are already described in detail above, and data on the substitution degree of Al atoms for the corresponding *d*-metal in *Me*C are listed in Tables 7 and 10.

The difference in the character of interaction between *Me*N and *Me*C with Al is illustrated in Fig. 22, where the microstructures of cBN–NbN–Al and cBN–NbC–Al composites sintered at different temperatures are presented. Thus, the bright white stripes on the SEM image of the composite of the cBN–NbC–Al system sintered at 1850 °C correspond to Nb atoms, which were released from the NbC lattice into Al solution. Similar bright white stripes are absent in SEM images of cBN–NbN–Al and cBN–NbC–Al composite sintered at higher temperatures (Fig. 22). The light grey stripes on all SEM images can be attributed to the products of the reaction — niobium borides.

SEM images of composites of cBN–ZrN–Al and cBN–ZrC–Al systems have a similar pattern at low sintering temperatures (Fig. 23).

Probably, the interaction of *Me*C with Al occurs by the vacancy mechanism as described in detail for TiC. However, this mechanism is not working in the case of *Me*N. That is why the crystal lattices of *Me*C are defective for *d*-metal (Table 7), while the crystal lattices of *Me*N are complete (Table 4).

Summing up, we can state that the interaction of components of the cBN–*Me*C–Al charge leads to the formation of carbonitrides of corresponding metal at high pressure. However, nitrogen atoms are not placed in 4*b* position along with carbon atoms but occupy a separate place in the internodes of the crystal lattice (Fig. 12). At certain sintering temperature, *Me*C carbides dissolve Al atoms in an amount that correlates with the breaking energy of *Me*–C bonds (Fig. 24).

It should also be noted that the calculated amount of excess nitrogen in TiCN of cBN–TiCN–Al composite and the amount of Al dissolved in it are close to values determined for TiC phase of cBN–TiC–Al composite (Figs. 19 and 24).

5. Conclusions

This paper presents and summarizes the results of a detailed and systematic XRD study of the crystal structure of *Me*N, *Me*C and TiCN phases, serving as the binders together with Al for PcBN composites of BL group of cBN–*Me*N–Al, cBN–*Me*C–Al, and cBN–*Me*CN–Al systems (with composition ratio of charge 60:35:5 vol.%) obtained by HPHT sintering. The XRD structural analysis presented in this article and recently published works [45, 46, 57–60] allows us to conclude the following features.

(1) The crystal structure of *Me*N, *Me*C, and TiCN phases of PcBN composites obtained belongs to a modified NaCl-type structural model, containing an additional position partially occupied by nitrogen atoms. This unique model can be considered as a new structural type of inorganic compound.

(2) The crystal structure of each *Me*N, *Me*C, and TiCN phase, existing in HPHT-sintered cBN–*Me*N–Al, cBN–*Me*C–Al, and cBN–*Me*CN–Al com-

posites was refined within the framework of a modified NaCl-type crystal lattice, revealing the occupation factors for:

• 4*a* position of the metal sublattice of *Me*C and TiCN structures occupied by *Me* or *Me*/Al atoms (under certain sintering modes);

• 4*b* positions of the non-metallic sublattice of *Me*N and *Me*C structures by nitrogen or carbon atoms;

• 24*e* position, which is additional to NaCl type structure by nitrogen atoms.

(3) Based on the structural-calculations' results, the composition of each of the *Me*N, *Me*C, and TiCN phases was determined. At that, we revealed as follows:

• diffusion of nitrogen accumulated in the initial charge, and released at cBN decomposition and during dissociation of *Me*N phases, leads to the formation of a surface nitrogen-enriched layer in HPHT sintered composites.

• at certain temperature regimes of HPHT sintering Al atoms of the charge are embedded in *Me*C crystal structures, forming substitutional solid solutions of corresponding metal; nitrogen atoms released during cBN decomposition, migrating along the sample, are placed either in the internodes of crystal lattice of these carbides, or in the vacancies available in its carbon sublattice;

• TiCN carbonitride manifests itself as a carbide at HPHT sintering, forming solid solutions with aluminium and nitrogen, the composition of which is close to the composition of a TiC-based solid solution;

• the temperature regions of existence and composition of $MeN_{1+\delta}$, *Me*CN and $Me_{1-x}Al_xCN$ solid solutions, existing in the products of HPHT sintering studied are determined.

It is shown that the studied features of *Me*N and *Me*C crystal structures are in a good agreement with existing theoretical assumptions on the solid-phase interaction of components with the participation of these carbides or nitrides. Namely:

The existence of positions for additional nitrogen atoms in the structures of *Me*N and carbides established by XRD is well described within the framework of the atomistic diffusion model, which controls the spontaneous formation of the Frenkel pairs from interstitial nitrogen atoms N(2) and lattice vacancies N(1) in nitrides (or vacancies of C atoms in carbides). More specifically, the dissociation of *Me*N located in the grains inside the sample mainly occurs by evaporation both at high and normal pressure. Diffusion flows of nitrogen atoms released in this case are directed from the middle of the sample towards its surface due to the temperature gradient in the reaction zone. Migrating, nitrogen atoms partially leave the composite in the form of N_2 gas and partially are intercepted by nitrides (the energy of the Me–N bonding is higher than the energy of the N–N bonding) with the formation of surface layers containing nitrogen-enriched

*Me*N phases. It is shown that the content of excess nitrogen accumulated in the *Me*N structure correlates with the enthalpy of their formation. The activation energy of nitrogen diffusion is determined by the amount of excess nitrogen increase in the HfN → TiN → VN → NbN series.

The formation of aluminium solid solutions at certain HPHT sintering regimes can be explained by the well-known mechanism of interaction of liquid Al with *Me*C at normal pressure, which consists in the release of *Me* atoms from the carbide lattice followed by the accumulation of vacancies in their metal sublattice. It is the gradual accumulation of vacancies, which is characteristic of *Me*C phases at low sintering temperatures according to the XRD study. Aluminium atoms from the HPHT reaction zone can penetrate the defective *Me*C lattice due to diffusion, and the released metal atoms will take part in the formation of MeB_2 diborides. It is shown that the amount of both aluminium and nitrogen atoms, which take part in the formation of solid solutions based on the initial *Me*C correlates with the energy of thermochemical dissociation of *Me*–C bonds.

We assume that similar structural transformations with the formation of phases with a modified NaCl-type crystal structure will be inherent in *Me*N and *Me*C, which exist in HPHT sintered PcBN composites with combined binders containing a mixture of these compounds.

In this paper, for the first time, an attempt was made to use the amount of excess nitrogen in surface *Me*N phases of cBN–*Me*N–Al composites determined by XRD structural analysis, to determine the main parameters of nitrogen diffusion (activation energy and atomic mobility) at HPHT sintering. Since the values obtained are compatible with theoretical data, we assume that the results of structural calculations can be applied to estimate the diffusion processes in cBN–*Me*N–Al composites of other compositions and sintering modes.

Acknowledgements. This study was financially supported by the Ministry of Education and Science of Ukraine within the agreements No. RN 14-2023 and No. 24БФ051-01 as well as by the National Research Foundation of Ukraine within the framework of the projects Nos. 2023.05/0007 and 2023.04/0139.

REFERENCES

1. G. Will, G. Nover, and J. von der Gönna, *J. Solid State Chem.*, **154**: 280285 (2000); https://doi.org/10.1006/jssc.2000.8850
2. F.R. Corrigan and F.P. Bundy, *J. Chem Phys.*, **63**, No. 9: 3812 (1975); https://doi.org/10.1063/1.431874
3. F. Klocke, *Manufacturing Processes 1: Turning, Milling, Drilling* (2011).
4. O.O. Kurakevych and V.L. Solozhenko, *Molecules*, **21**, No. 10: 1399 (2016); https://doi.org/10.3390/molecules21101399
5. V.L. Solozhenko, I.A. Petrusha, and A.A. Svirid, *High Press. Res.*, **15**: 95 (1996); https://doi.org/10.1080/08957959608240463

6. S.N. Dub and I.A. Petrusha, *High Press. Res.*, **26**, No. 2: 71 (2006); https://doi.org/10.1080/08957950600764239
7. N.P. Bezhenar, S.M. Konoval, S.A. Bozhko, N.N. Beljavina, and V.Ya. Markiv, *High Press. Phys. Eng.*, **19**, No. 2: 41 (2009); http://jnas.nbuv.gov.ua/article/UJRN-0000118328
8. M.P. Bezhenar, M.H. Loshak, O.O. Shulzhenko, S.M. Konoval, L.I. Aleksandrova, S.A. Bozhko, and N.M. Biliavyna, *Porodorazrushayushchiy i Metalloobrabatyvayushchiy Instrument — Tekhnika i Tekhnologiya ego Izgotovleniya i Primeneniya*, No. 11: 164 (2008) (in Russian).
9. M.P. Bezhenar, S.M. Konoval, S.A. Bozhko, M.G. Loshak, L.I. Aleksandrova, M.I. Zaika, P.A. Nagornyi, and H.M. Bilyavina, *J. Superhard Materials*, **32**: 1 (2010); https://doi.org/10.3103/S1063457610010016
10. M.P. Bezhenar, Ya.M. Romanenko, S.M. Konoval, T.A. Harbuz, V.Y. Zelenyn, M.A. Poleshchuk, and Yu.A. Nykytiuk, *Porodorazrushayushchiy i Metalloobrabatyvayushchiy Instrument — Tekhnika i Tekhnologiya ego Izgotovleniya i Primeneniya*, No. 19: 184 (2016) (in Russian).
11. S.A. Klymenko, M.Yu. Kopeikyna, and A.O. Chumak, *Suchasni Tekhnologii v Mashynobuduvanni*, No. 12: 54 (2017) (in Ukrainian).
12. S.A. Klymenko, Yu.O. Melniichuk, Yu.O. Mukovoz, M.Yu. Kopieikina, I.A. Petrusha, and O.S. Osypov, *Deklaratsiinyi Patent Ukrainy No. 70820 A, Sposib Mekhanichnoi Obrobky. Bulletin 'Promyslova Vlasnist'*, **10**: 54 (2004) (in Ukrainian).
13. A. McKie, J. Winzer, I. Sigalas, M. Herrmann, L. Weiler, J. Rudel, and N. Can, *Ceram. Int.*, **37**, No. 1: 1 (2011); https://doi.org/10.1016/j.ceramint.2010.07.034
14. V. Bushlya, F. Lenrick, J.-E. Stehl, and R. M'Saoubi, *CIRP Ann.*, **67**, No. 1: 79 (2018); https://doi.org/10.1016/j.cirp.2018.03.011
15. R. M'Saoubi, M.P. Johansson, and J.M. Andersson, *Wear*, **302**, Nos. 1–2: 1219 (2013); https://doi.org/10.1016/j.wear.2013.01.074
16. V. Bushlya, J. Zhou, P. Avdovic, and J.-E. Ståhl, *Int. J. Adv. Manuf. Technol.*, **66**, Nos. 9–12: 1083 (2013); https://doi.org/10.1007/s00170-013-4899-8
17. K. Sobiyi, I. Sigalas, G. Akdogan, and Y. Turan, *Int. J. Adv. Manuf. Technol.*, **77**, Nos. 5–8: 861 (2015); https://doi.org/10.1007/s00170-014-6506-z
18. V.M. Bushlya, O.A. Gutnichenko, J.M. Zhou, J.-E. Stehl, and S. Gunnarsson, *J. Superhard Mater.*, **36**, No. 1: 49 (2014); https://doi.org/10.3103/S1063457614010080
19. V. Bushlya, O. Gutnichenko, J. Zhou, P. Avdovic, and J.-E. Stehl, *Mach. Sci. Technol.*, **17**, No. 4: 497 (2013); https://doi.org/10.1080/10910344.2013.806105
20. J. Angseryd and H.O. Andren, *Wear*, **271**, Nos. 9–10: 2610 (2011); https://doi.org/10.1016/j.wear.2010.11.059
21. P. Klimczyk, E. Benko, K. Lawniczak-Jablonska, E. Piskorska, M. Heinonen, A. Ormaniec, W. Gorczynska-Zawislan, and V.S. Urbanovich, *J. Alloys Compd.*, **382**, Nos. 1–2: 195 (2004); https://doi.org/10.1016/j.jallcom.2004.04.140
22. J. Angseryd, E. Coronel, M. Elfwing, E. Olsson, and H.O. Andren, *Wear*, **267**, Nos. 5–8: 1031 (2009); https://doi.org/10.1016/j.wear.2008.12.075

23. L. Zhang, F. Lin, Z. Lv, C. Xu, X. He, W. Wang, and L. Xia, *Int. J. Refract. Met. Hard Mater.*, **50**: 221 (2015); https://doi.org/10.1016/j.ijrmhm.2015.01.015
24. K.V. Slipchenko, I.A. Petrusha, V.Z. Turkevich, V.M. Bushlya, and J.-E. Stahl, *Metallofiz. Noveishie Tekhnol.*, **40**, No. 8: 1081 (2018) (in Ukrainian); https://doi.org/10.15407/mfint.40.08.1081
25. K. Slipchenko, D. Stratiichuk, N. Belyavina, V. Turkevich, V. Bushlya, J.E. Stahl, *9th Swedish Production Symposium—SPS 2020*, **13**: 428 (2020); https://doi.org/10.3233/ATDE200180
26. K. Slipchenko, V. Turkevich, I. Petrusha, V. Bushlya, and J.-E. Stehl, *Procedia Manuf.*, **25**: 322 (2018); https://doi.org/10.1016/j.promfg.2018.06.090
27. M.P. Bezhenar, G.S. Oleinik, S.A. Bozhko, T.O. Garbuz, and S.M. Konoval, *J. Superhard Mater.*, **31**, No. 6: 357 (2009); https://doi.org/10.3103/S106345760906001X
28. K. Slipchenko, V. Bushlya, D. Stratiichuk, I. Petrusha, A. Can, V. Turkevich, and F. Lenrick, *J. Eur. Ceram. Society*, **42**, No. 11: 4513 (2022); https://doi.org/10.1016/j.jeurceramsoc.2022.04.022
29. X.Z. Rong, T. Tsurumi, O. Fukunaga, and T. Yano, *Diam. Relat. Mater.*, **11**, No. 2: 280 (2002); https://doi.org/10.1016/S0925-9635(01)00692-6
30. E. Benko, J.S. Stanisław, B. Krylicka, A. Wyczesany, and T.L. Barr, *Diam. Relat. Mater.*, **8**, No. 10: 1838 (1999); https://doi.org/10.1016/S0925-9635(99)00131-4
31. H. Xie, F. Deng, H. Wang, J. Liu, S. Han, and F. Feng, *J. Refract. Metals Hard Mater.*, **89**: 105209 (2020); https://doi.org/10.1016/j.ijrmhm.2020.105209
32. S.Y. Chiou, S.F. Ou, Y.G. Jang, and K.L. Ou, *Ceram. Int.*, **39**, No. 6: 7205 (2013); https://doi.org/10.1016/j.ceramint.2013.02.066
33. K. Slipchenko, V. Bushlya, D. Stratiichuk, V. Turkevich, and J.-E. Ståhl, *Procedia CIRP*, **101**: 254 (2021); https://doi.org/10.1016/j.procir.2020.10.005
34. K.V. Slipchenko, V.Z. Turkevich, V.M. Bushlya, and J.-E. Stehl, *Rock. Destr. Met. Tools — Tech. Technol. Tool. Prod. Appl.*, No. 22: 254 (2019).
35. K.V. Slipchenko, I.A. Petrusha, V.Z. Turkevich, V.M. Bushlya, and J.-E. Stehl, Rock. *Destr. Met. Tools — Tech. Technol. Tool. Prod. Appl.*, No. 21: 275 (2018).
36. K.V. Slipchenko, I.A. Petrusha, D.A. Stratiichuk, and V.Z. Turkevych, *J. Superhard Mater.*, **40**: 226 (2018); https://doi.org/10.3103/S1063457618030115
37. K.V. Slipchenko, V.Z. Turkevich, V.M. Bushlya, and J.-E. Ståhl (2019), *Tooling Materials Science*, No. 22: 254 (2019); http://jnas.nbuv.gov.ua/article/UJRN-0001089259
38. K.V. Slipchenko, I.A. Petrusha, V.Z. Turkevich, D.A. Stratiichuk, V.M. Slipchenko, N.M. Bilyavina, D.V. Turkevich, V.M. Bushlya, and J.-E. Ståhl, *Metallofiz. Noveishie Tekhnol.*, **41**, No. 12: 1599 (2019) (in Ukrainian); https://doi.org/10.15407/mfint.41.12.1599
39. K.V. Slipchenko, D.A. Stratiichuk, V.Z. Turkevich, N.M. Bilyavyna, V.M. Bushlya, and J.-E. Ståhl, *J. Superhard Mater.*, **42**, No. 4: 229 (2020); https://doi.org/10.3103/S1063457620040103
40. D.A. Stratiichuk, V.Z. Turkevich, K.V. Slipchenko, and V.M. Bushlya, *Dopov. Nac. Akad. Nauk Ukr.*, No. 9: 38 (2020) (in Ukrainian);

https://doi.org/10.15407/dopovidi2020.09.038
41. D.A. Stratiichuk, V.Z. Turkevich, K.V. Slipchenko, Yu.O. Melniichuk, and D.V. Turkevich, *Tooling Materials Science*, No. 23: 194 (2020).
42. D.A. Stratiichuk, V.Z. Turkevich, K.V. Slipchenko, V.M. Bushlya, and N.M. Bilyavyna, *Dopov. Nac. Akad. Nauk Ukr.*, No. 2: 37 (2020) (in Ukrainian); https://doi.org/10.15407/dopovidi2020.02.037
43. K.V. Slipchenko, D.A. Stratiichuk, V.Z. Turkevich, N.M. Belyavina, V.M. Bushlya, and J.-E. Stehl, *J. Superhard Mater.*, **42**: 51 (2020); https://doi.org/10.3103/S1063457620020112
44. M. Dashevskyi, O. Boshko, O. Nakonechna, and N. Belyavina, *Metallofiz. Noveishie Tekhnol.*, **39** No. 4: 541 (2017); https://doi.org/10.15407/mfint.39.04.0541
45. N.N. Belyavina, D.A. Stratiichuk, O.I. Nakonechna, T.G. Avramenko, A.M. Kuryliuk, and V.Z. Turkevich, *Dopov. Nac. Akad. Nauk Ukr.*, No. 2: 58 (2022) (in Ukrainian); https://doi.org/10.15407/dopovidi2022.02.058
46. N.M. Belyavina, V.Z. Turkevich, A.M. Kuryliuk, D.A. Stratiichuk, O.I. Nakonechna, P.P. Kogutyuk, and L.P. Stasuk, *Dopov. Nac. Akad. Nauk Ukr.*, No. 1: 20 (2024) (in Ukrainian); https://doi.org/10.15407/dopovidi2024.01.020
47. T.G. Avramenko, A.M. Kuryliuk, O.I. Nakonechna, and N.N. Belyavina, *Metallofiz. Noveishie Tekhnol.*, **44**, No. 6: 713 (2022); https://doi.org/10.15407/mfint.44.06.0713
48. W. Lengauer, *J. Phys. Chem. Sol.*, **52**. No. 2: 393(1991); https://doi.org/10.1016/0022-3697(91)90089-I
49. E. Penilla and J. Wang, *J. Nanomater.*, **2008**: 1 (2008); https://doi.org/10.1155/2008/267161
50. R. Fix, R.G. Gordon, and D.M. Hoffman, *Chem. Mater.*, **5**, No. 5: 614 (1993); https://doi.org/10.1021/cm00029a007
51. D.G. Sangiovanni, B. Alling, P. Steneteg, L. Hultman, and I.A. Abrikosov, *Phys. Rev. B*, **91**, No. 5: 054301 (2015); https://doi.org/10.1103/PhysRevB.91.054301
52. S. Yu, Q. Zeng, A.R. Oganov, G. Frapper, and L. Zhang, *Phys. Chem. Chem. Phys.*, **17**, No. 17: 11763 (2015); https://doi.org/10.1039/c5cp00156k
53. H. Yang, Z. Qian, H.Chen, X. Zhao, G. Han, W. Du, X. Nie, K. Zhao, G. Liu, Q. Sun, T. Gao, J. Zhou, J. Nie, and X. Liu, *Acta Mater.*, **233**: 117977 (2022); https://doi.org/10.1016/j.actamat.2022.117977
54. O.I. Nakonechna, M.M. Dashevskyi, O.I. Boshko, V.V. Zavodyannyi, and N.N. Belyavina, *Prog. Phys. Met.*, **20**, No. 1: 5 (2019); https://doi.org/10.15407/ufm.20.01.005
55. A. Sevy, D.J. Matthew, and M.D. Morse, *J. Chem. Phys.*, **149**, No. 4: 044306 (2018); https://doi.org/10.1063/1.5041422
56. W. Lengauer and A. Eder, *Nitrides: Transition Metal Solid-State Chemistry. Encyclopedia of Inorganic Chemistry. First Edition* (Wiley: 2006), p. 3515; https://doi.org/10.1002/0470862106.ia156
57. N.M. Belyavina,V.Z. Turkevich, A.M. Kuryliuk, D.A. Stratiichuk, L.P. Stasuk, O.I. Nakonechna, and P.P. Kogutyuk, *Dopov. Nac. Akad. Nauk Ukr.*, No. 3: 40 (2023); https://doi.org/10.1021/cm00029a007
58. N.M. Belyavina, D.A. Stratiichuk, A.M. Kuryliuk, V.Z. Turkevich, O.I. Nakonechna, P.P. Kogutyuk, and L.P. Stasuk, *J. Nano- Electron. Phys.*, **15**, No. 3: 03030 (2023);

https://doi.org/10.21272/jnep.16(2).02013
59. A.M. Kuryliuk, V.Z. Turkevich, N.M. Belyavina, D.A. Stratiichuk, O.I. Nakonechna, and P.P. Kogutyuk, *The 9th Int. Conf. 'Physics of Disordered Systems' (PDS'2023) (19–20 September 2023, Lviv, Ukraine)*, p. 60.
60. N.M. Belyavina, V.Z. Turkevich, D.A. Stratiichuk, A.M. Kuryliuk, and O.I. Nakonechna, *J. Nano- Electron. Phys.*, **16**, No. 2: 02013 (2024); https://doi.org/10.2127 2/jnep.16(2).02013

Received 01.07.2024
Final version 08.11.2024

Н.М. Білявина[1], *В.З. Туркевич*[2],
Д.А. Стратійчук[2], *А.М. Курилюк*[1], *О.І. Наконечна*[1]
[1] Київський національний університет імені Тараса Шевченка, вул. Володимирська, 64/13, 01601 Київ, Україна
[2] Інститут надтвердих матеріалів ім. В.М. Бакуля НАН України, вул. Автозаводська, 2, 04074 Київ, Україна

ЩОДО УТВОРЕННЯ ТВЕРДИХ РОЗЧИНІВ ЗА ТЕРМОБАРИЧНОГО СПІКАННЯ PcBN-КОМПОЗИТІВ СИСТЕМ cBN–*Me*N–Al і cBN–*Me*C–Al

Методом рентгенівської дифракції докладно вивчено серію полікристалічних кубічних композитів нітриду Бору (PcBN) систем cBN–{TiN, ZrN, HfN, VN, NbN}–Al і cBN–{TiC, ZrC, HfC, VC, NbC, TaC}–Al (зі складом шихти 60:35:5 об.%), спечених за високих тисків і температур (HPHT): 7,7 ГПа і 1600–2450 °C. Показано, що кристалічна структура кожного нітриду *Me*N і карбіду *Me*C (*Me* = Ti, Zr, Hf, V, Nb, Ta), що є у цих композитах, належить до модифікованої структури типу NaCl з додатковою позицією для атомів Нітрогену, що зумовлює акумуляцію надлишку атомів N у приповерхневих шарах композитів. За певних температурних режимів HPHT-спікання Алюміній шихти занурюється в кристалічні структури карбідів *Me*C, утворюючи тверді розчини заміщення на основі відповідного металу *Me*. Визначено температурні області існування та склад твердих розчинів $MeN_{1+\delta}$, $MeCN_{\delta}$, $Me_{1-x}Al_xCN_{\delta}$ у досліджених продуктах HPHT-спікання. Встановлені особливості кристалічних структур цих твердих розчинів цілком відповідають наявним теоретичним уявленням про процеси, що описують характер твердофазної взаємодії компонентів шихти за її спікання. Так, накопичення Нітрогену у *Me*N і *Me*C описується в рамках моделі атомістичного дифузійного процесу. З використанням даних про надлишок N у нітридах як опорних значень визначено основні параметри процесу дифузії (енергію активації та константу швидкості) Нітрогену в композитах cBN–{TiN, HfN, VN, NbN}–Al. Утворення за певних режимів HPHT-спікання твердих розчинів Алюмінію пояснюється механізмом взаємодії рідкого алюмінію з карбідами *Me*C, якому передує активне утворення вакансій у металевій підґратці цих карбідів. Методологічно вперше використано дані рентгеноструктурного аналізу для визначення основних параметрів процесу міграції атомів N у процесі HPHT-спікання композита з його середини на поверхню.

Ключові слова: кубічний нітрид Бору (cBN), композит, мононітрид, монокарбід, рентгенівська дифракція, дифузія.